Breast Cancer Imaging: State of the Art 2011—Poster Abstracts

SNM and the SNM Center for Molecular Imaging Innovation and Translation (CMIIT) are sponsoring a symposium designed to help disseminate the latest research on the diagnosis, staging, and treatment of patients with breast cancer with a specific focus on the integration of molecular imaging with standard diagnostic radiology. The symposium Breast Cancer Imaging: State of the Art 2011 will be held this month at the National Institutes of Health (NIH) and will include a series of lectures from invited experts in the field, panel discussions, and a poster session. In this special section of *JNM*, we are publishing the 37 original abstracts selected for poster presentation at this symposium.

See www.snm.org/breast2011 for information on the speakers and agenda. This conference is designed to build on successful symposia on cardiovascular molecular imaging held at NIH in May 2009 (*J Nucl Med.* 2009;50:656–665) and molecular neuroimaging held at NIH in May, 2010 (*J Nucl Med.* 2010;51:826–835).

The speaker roster includes expert diagnostic radiologists, nuclear medicine physicians and basic scientists, medical oncologists, surgeons, economists, and radiation oncologists. During the two-day meeting, the current state of imaging in breast cancer will be reviewed—from the screening mammography controversy and advanced screening technology to local and distant staging and response to treatment.

The abstracts presented here represent some of the most interesting ideas in molecular imaging research as applied to the diagnosis, staging, and treatment of patients with breast cancer. We have put particular emphasis on participation by junior scientists. The first section contains those abstracts selected to receive Young Investigator Travel Awards* sponsored by the Society of Radiopharmaceutical Sciences, Academy of Molecular Imaging, and the Society for Molecular Imaging.

Maxine Jochelson, MD
Memorial Sloan-Kettering Cancer Center
PI and Organizing Committee Member

Abstract Reviewers

*Abstracts are listed alphabetically by first author within each section.

SECTION 1

Young Investigator Travel Award Winners

1***

Quantification of early response to neoadjuvant chemotherapy in breast cancer: initial studies in humans using a high resolution PET/CT scanner. A. Ferrero[1], A.J. Chaudhari[2], S.L. Bowen[3], K. Yang[2], K.K. Lindfors[2], J.M. Boone[2], S.R. Martines[4], R.D. Badawi[2]; 1. Department of Biomedical Engineering, UC Davis Medical Center, Sacramento, CA; 2. Department of Radiology, UC Davis Medical Center, Sacramento, CA; 3. Department of Radiology, MGH, Charlestown, MA; 4. Department of Surgical Oncology, UC Davis School of Medicine, Sacramento, CA

Objectives: To evaluate the role of a high resolution PET/CT dedicated breast scanner for the quantitative assessment of early response to neoadjuvant chemotherapy (NAC) in human breast cancer patients. **Methods:** A high resolution PET/CT dedicated breast scanner has been built at our institution, the first of its kind. The patient's breast is imaged by this system in the pendant position, with no compression applied. Data corrections, with the exception of scatter correction, have been applied to raw PET signals to obtain semiquantitative images. To date, three patients with invasive breast cancer (ductal or lobular) who were candidates for radical mastectomy have been scanned with 18F-FDG-PET/CT at baseline and at the end of the first cycle of NAC. Two of these patients have also been scanned at the conclusion of treatment, before surgery. Histopathological analyses have been performed on the excised specimens. **Results:** For patient 1 (47f), with invasive ductal carcinoma, a reduction in normalized (by weight and injected dose) maximum lesion intensity, Imax, compared to baseline of 26% and 60%, was observed at the end of the first cycle of NAC and immediately before surgery, respectively. Histopathology confirmed positive residual ductal carcinoma, indicating the patient was not a complete responder to NAC from both a pathological and a metabolical standpoint. For patients 2 (48f) and 3 (56f) the lesion was too posterior (i.e., too close to the chest wall) to be included within the PET field of view at every time point in the study. **Conclusions:** These initial findings indicate that high resolution, quantitative PET/CT was able to predict pathological response to NAC treatment at the end of the first cycle of chemotherapy, for this initial patient. Due to the scanner design, however, lesions close (i.e. <2 cm) to the chest wall are very difficult to be imaged. This is a 30 patient study, and recruitment is ongoing.

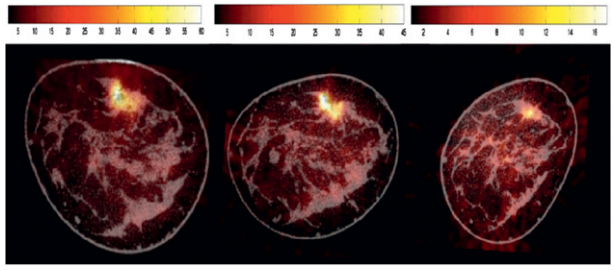

FIGURE 1.

2*

MicroSPECT/CT imaging of EGFR-positive tumor xenografts in athymic mice with 111In-Bn-DTPA-nimotuzumab with/without nuclear localization sequence (NLS) peptide modification. H.A. Fonge[1], R.M. Reilly[1], A. Fasih[1], J. Leyton[1], C. Allen[1]; 1. University of Toronto, Toronto, Canada

Objectives: 111In-Bn-DTPA-NLS-nimotuzumab (Nmab) is an Auger electron-emitting radioimmunotherapeutic (RIT) agent harbouring NLS peptides under investigation for EGFR-positive breast cancer (BC). Our aim was to compare the tumor and normal tissue distribution of 111In-Bn-DTPA-Nmab with/without NLS peptides in athymic mice bearing EGFR-positive s.c. human BC xenografts. **Methods:** EGFR affinity was measured in a direct binding assay using MDA-MB-468 cells. Mice with s.c. MDA-MB-468, MDA-MB-231 or MCF-7 BC xenografts with 106, 105 or 104 EGFR/cell, respectively, were injected i.v. with 16 – 20 MBq (10 μg) of 111In-Bn-DTPA-Nmab or 111In-Bn-DTPA-NLS-Nmab. Mice with trastuzumab (Herceptin)-resistant TrR1 and TrR2 tumors (105 EGFR/cell) were also studied. Specificity was evaluated by pre-dosing with 1 mg Nmab or using irrelevant 111In-Bn-DTPA-rituximab (anti-CD20). Pharmacokinetic, biodistribution and microSPECT/CT studies were performed up to 72 h p.i. **Results:** EGFR affinity was preserved after Bn-DTPA and NLS conjugation (Kd = 13.9 vs. 10.8 nM for 111In-Bn-DTPA-Nmab vs. 111In-Bn-DTPA-NLS-Nmab, respectively). NLS modification resulted in faster elimination of 111In-Bn-DTPA-Nmab (4.3 ± 1.9 % vs. 29.6 ± 1.8 % i.d./g in the blood at 72 h) and lower tumor uptake (8.6 ± 2.2 % vs. 25.3 ± 6.4 % i.d./g in MDA-MB-468 tumors at 48 h). Liver uptake was higher for 111In-Bn-DTPA-NLS-Nmab than for 111In-Bn-DTPA-Nmab (8.8 ± 2.8 % vs. 4.2 ± 0.5 % i.d./g at 48 h). Tumor uptake of 111In-Bn-DTPA-Nmab and 111In-Bn-DTPA-NLS-Nmab was proportional to EGFR density and was significantly higher than 111In-Bn-DTPA-rituximab (except for MCF-7 tumors). **Conclusions:** MicroSPECT/CT was valuable for comparing the tumor and normal tissue distribution of 111In-Bn-DTPA-Nmab and 111In-Bn-DTPA-NLS-Nmab. Tumor EGFR expression levels can be differentiated by imaging and this may be helpful to select patients for Auger electron RIT. Supported by a grant from the Canadian Breast Cancer Research Alliance, the Ontario Institute of Cancer Research and YM BioSciences, Inc.

3***

Detectors for the next generation of high resolution dedicated PET/CT scanners for breast imaging. F. Godinez[1], A. Ferrero[1], A.J. Chaudhari[1], R.D. Badawi[1]; 1. University of California Davis, Davis, CA

Objectives: A high resolution PET/CT dedicated breast scanner was built at our institution, the first of its kind. Initial clinical scans showed that the current prototype suffers from some limitations, including moderate spatial resolution (~2.5 mm), lack of depth of interaction (DOI) information, which affects spatial resolution uniformity across the field of view (FOV), and poor energy resolution. The aim of this study is to design and test new detectors to address these limitations in a second generation of scanners. **Methods:** Two detectors have been designed and built, with a third under construction. The completed detectors are based on a 14x14 array of 1.5x1.5x20 mm^3 unpolished LSO scintillation crystals, with each element coated in a 50 micron layer of reflective material (Toray™). The first detector is read out from one end using a position sensitive photomultiplier tube (PSPMT) (Hamamatsu C-12 8900). The second detector is read out from both ends using a similar PSPMT and an avalanche photodiode (PSAPD) (RMD Inc, Watertown, MA) to enable acquisition of DOI information. The third detector is based on a 36x36 array of 0.5x0.5x20 mm^3 unpolished LSO

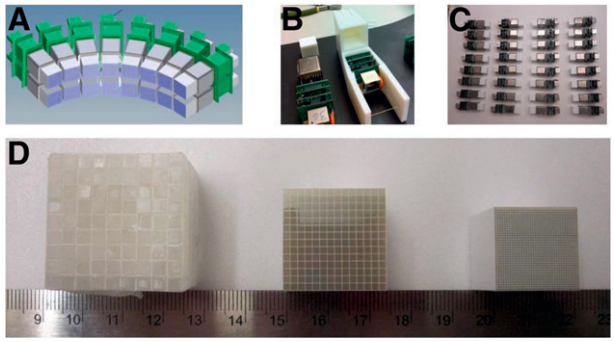

FIGURE 1. A) Detector head design layout for non-DOI prototype breast scanner. B) Detector components and gantry support modules for non-DOI scanner. C) Detector components (arrays, pmts, pre-amp stacks) awaiting gantry mounting. D) Left: LSO array for the existing breast PET/CT (3.3 mm pitch). Center: 1.5 mm pitch LSO array. Right: 0.5 mm pitch ultra high-resolution array.

*Travel award sponsored by the Society of Radiopharmaceutical Sciences.
**Travel award sponsored by the Academy of Molecular Imaging.
***Travel award sponsored by the Society for Molecular Imaging.

crystals and will also have dual ended readout. It will be used for limited field-of-view ultra-high resolution molecular imaging of the breast. Nuclear Instrumentation Modules (NIM) were used to characterize the detectors' performances in terms of timing, intrinsic spatial resolution and energy resolution, as well as DOI resolution for the module with the dual ended readout. Measurements with the PSAPD were performed at a temperature of 10°C. **Results:** We measured a timing resolution of 2.4 ns, an energy resolution of 24% and 16% with the completed single and dual ended readout detectors, respectively. The intrinsic spatial resolution was measured to average 1.3 mm for crystals in the array central row of the single-ended readout detector. The average DOI resolution was measured to be 2.9 mm of the dual-ended readout detector. **Conclusions:** These preliminary results show good promise regarding the possibilities of building second generation breast PET/CT scanners with significantly increased spatial resolution. Designs for and progress in construction of fully operational prototype scanners using these detectors will also be presented.

4**

Molecular breast imaging (MBI) in monitoring treatment response to neoadjuvant chemotherapy. C.B. Hruska[1], D.L. Wahner-Roedler[1], J.C. Boughey[1], A.L. Conners[1], C.L. Tortorelli[1], R. Maxwell[1], M.K. O'Connor[1], D.J. Rhodes[1]; 1. Mayo Clinic, Rochester, MN

Objectives: The purpose of this study was to assess the value of molecular breast imaging (MBI) for monitoring treatment response in patients with breast cancer undergoing neoadjuvant chemotherapy (NC). **Methods:** Between December 2009 and August 2010, ten patients with breast cancer consented to undergo MBI prior to initiation of NC, 3–5 weeks into NC, and at completion of NC prior to breast cancer surgery. MBI was performed using a dedicated dual-head CZT-based gamma camera system after injection of 296 MBq Tc-99m sestamibi. Tumor size was characterized by the longest diameter measured on MBI and pathology. **Results:** The median age of 10 patients was 50 years (r, 42–67). Median tumor size based on MBI interpretation was 3.5 cm (range 2.2–7.5) prior to NC, 1.8 cm (range 0–5.2) at 3–5 weeks into NC, and 0.6 cm (range 0–8.4) at completion of NC. The median size of invasive cancer as determined by pathology at time of breast cancer surgery was 1.0 cm (range 0–8.5). In 5 patients, the final MBI was negative and the pathology was negative for invasive cancer, although in 2 of these patients, a small area of DCIS was identified on pathology that was not detected on MBI. In the remaining 5 patients, final tumor size based on MBI correlated within a 1–9 mm range with final tumor size on pathology. Interestingly, tumor size decreased initially after NC in 2 patients (#4, #5), but at completion of NC the tumors of these 2 patients were found to be of the same/larger size than pretreatment. **Conclusions:** Based on these preliminary data, response to NC in patients with breast cancer can be adequately monitored with MBI. Size of tumor on MBI after completion of NC correlates well with pathologic findings at surgery and may be useful to guide surgical choices.

5***

Integrin targeted phage as positron emission tomography (PET) agent: potential for breast cancer imaging. Z. Li[1], Q. Jin[2], C. Huang[1], L. Chen[2], L. Yap[1], P.S. Conti[1]; 1. University of Southern California, Los Angeles, CA; 2. Argonne National Laboratory, Argonne, IL

Objectives: The recent advancement of nanotechnology has provided unprecedented opportunities for the development of nanoparticle enabled technologies for detecting and treating cancer. However, applications of these nanotechniques were limited by the potential nanotoxicity and the lack of well controlled surface modification method. The objective of this research is to construct a PET trackable platform based on phage particles, which are physically well characterized, trackable after surface modification, biocompatible and biodegradable, nonpathogenic, and dictate their own target specific production. **Methods:** In our approach, we constructed an integrin αvβ3 targeted phage particle for PET imaging by expressing multiple RGD peptides on its surface. A bifunctional chelator (BFC) 1,4,7,10-tetraazadodecane-N,N',N",N"'-tetraacetic acid (DOTA) or AmBaSar was then conjugated to the phage surface for 64Cu2+ chelation. After 64Cu radiolabeling, microPET imaging was performed in a U87MG tumor model, and the receptor specificity was confirmed by blocking experiments. **Results:** The phage-RGD demonstrated target specificity based on an ELISA experiment. According to the TEM images, the morphology of the phage was unchanged after the modification with BFCs. The labeling yield was 25 ± 4% for 64Cu-DOTA-phage-RGD and 46 ± 5% for 64Cu-Sarphage-RGD, respectively. At the 1 h time point, 64Cu-DOTA-phage-RGD and 64Cu-Sar-phage-RGD have comparable tumor uptake (~ 8%ID/g). However, 64Cu-Sar-phage-RGD showed significantly higher tumor uptake (13.2 ± 1.5 %ID/g, $P<0.05$) at late time points compared with 64Cu-DOTAphage-RGD (10 ± 1.2%ID/g). 64Cu-Sar-phage-RGD also demonstrated significantly lower liver uptake, which could be attributed to the stability difference between two chelators. There is no significant difference between the two tracers regarding the uptake in kidney and muscle at all time points tested. In order to confirm the receptor specificity, a blocking experiment was performed. In the RGD blocking experiment, the cold RGD peptide was injected 2 min before the administration of 64Cu-Sar-phage-RGD. Tumor uptake was partially blocked at the 1 h time point. A phage-RGD particle was also used as the competitive ligand. In this case, the tumor uptake was significantly reduced, and the value was kept at low level consistently. **Conclusion:** Integrin αvβ3 has served as an important target for breast cancer imaging and targeted therapy. In this report, we constructed an integrin αvβ3 targeted platform based on phage particles that could also be trackable with PET. We also demonstrated that the choice of chelator could have a significant impact on imaging results. Moreover, these newly developed agents hold great therapeutic potential due to their high carrying capacity and superior targeted delivery ability obtained through polyvalency effect. The method established in this research may be applicable to other receptor/ligand systems for theranostic agent construction, which could have an immediate and profound impact on the field of imaging/therapy and lay the foundation for the construction of next generation cancer specific theranostic agents.

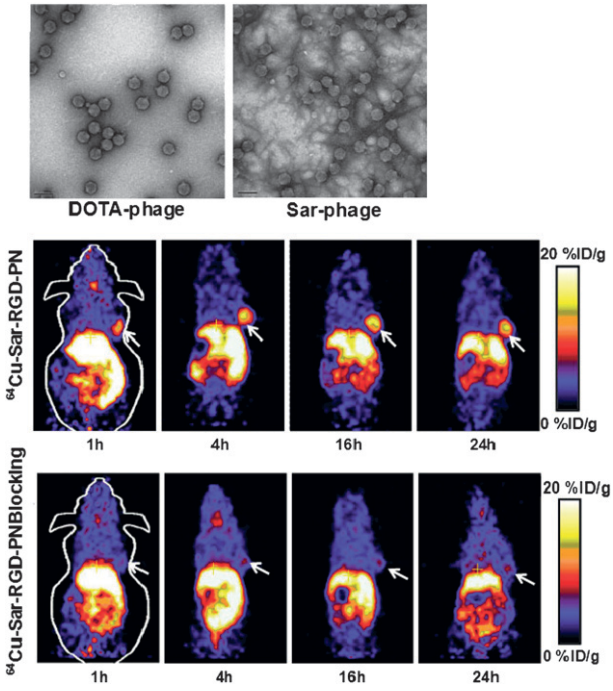

FIGURE 1.

6*

124I-PUH71 PET detects upregulated HSP90 breast cancer xenografts. C.A. Roney[1], K. Pillarsetty[1], E. Caldas-Lopes[1], T. Taldone[1], G. Chiosis[1], J.S. Lewis[1]; 1. Memorial Sloan-Kettering Cancer Center, New York, NY

*Travel award sponsored by the Society of Radiopharmaceutical Sciences.
***Travel award sponsored by the Society for Molecular Imaging.

Objectives: In 2010, nearly 40,000 women are estimated to die from breast cancer in the U.S. Early detection facilitates management and treatment. The molecular chaperone HSP90, an important therapeutic target in cancer, controls translocation of heat shock factor-1 (HSF-1), and organizes the activity, turnover and trafficking of aberrant proteins1-3. ATP/ADP regulates HSP90 activity, and in doing so, adopts a unique bent shape. This conformation was implemented in designing a novel purine scaffold class of ligands (PU-class) with nanomolar affinity for HSP90. Human xenograft MDA-MB-468 breast tumor cells were implanted into the mammary fat pad of female athymic nude mice. Two PU-derivatives (HSP90 inhibitors), PU-H71 and PU-DZ13, were radiolabeled with 124I, administered intravenously, and evaluated by *in vivo* positron emission tomography (PET), to validate HSP90 upregulation and tumor localization. The objective of this study was to establish breast cancer detection in the MDA-MB-468 model using novel PU-HSP90 inhibitors by *in vivo* small animal PET. **Methods:** Human triple negative breast cancer (TNBC) cells (MDA-MB-468) were cultured in a 1:1 mixture of Dulbecco's Modified Eagle medium/F-12 medium, supplemented with 10% heat inactivated FCS, 2.0 mM glutamine, non-essential amino acids, 100 U/mL penicillin, and 100 U/mL streptomycin (37°C, 5% CO2). Cells were harvested and passaged weekly in 0.25% trypsin/0.53 mmol EDTA in Hank's Buffered Salt Solution (without calcium and magnesium). Using a 20-gauge needle, 5x106 cells were implanted by s.c. injection (in a 200 µL cell suspension of 1:1 fresh media/BD Matrigel) into the left mammary fat pad of female athymic nude mice (N=10, 6-8 weeks old); tumors grew to 6.5-7.0 mm (21-25 days). HSP90 inhibitors were synthesized as previously reported. PU-H71 and PU-DZ13 were radiolabeled with 4 mCi (148 MBq) 124I each (Chloramine T method of radioiodination). The radiochemical yields were 31% (124IDZ13) and 60% (124I-H71); radiochemical purity (>98%) was confirmed by HPLC. For *in vivo* administration, the 124IPU-compounds were dissolved in PBS (pH 7.4); mice were pre-treated with 5% potassium iodide (KI) solution 24-48 hours prior to imaging to block thyroid uptake of iodine. 124I-PET imaged drug uptake of PU-H71 (N=5) and PU-DZ13 (N=5) at 1, 4, 12, 24, 48, and 72 hours. *in vivo* biodistribution was performed separately at the imaging time points to assess drug pharmacokinetics. **Results:** Both 124I-PUH71 and 124I-DZ13 accurately discriminated MDA-MB-468 tumors on *in vivo* PET. The inhibitor 124I-DZ13 had less nonspecific uptake by abdominal organs; tumor-to-blood ratio was 0.56 at one hour and 0.96 at 72 hours. Regions of interest (ROI) were drawn around the tumor volume, and the %ID/g was determined using the ASIpro imaging software. The %ID/g was lower at each time point for 124I-DZ13 versus 124I-PUH71 (e.g., 0.0489 ± 0.018 versus 0.0630 ± 0.018 at 24h), suggesting 124I-DZ13 was a better imaging agent. **Conclusions:** 124I-PUH71 and 124I-DZ13 target HSP90 overexpression in MDA-MB-468 xenograft mice, and are viable agents in the detection of breast cancer by *in vivo* small animal PET. The clinical implications of these drug targets are improved sensitivity in diagnostic imaging.

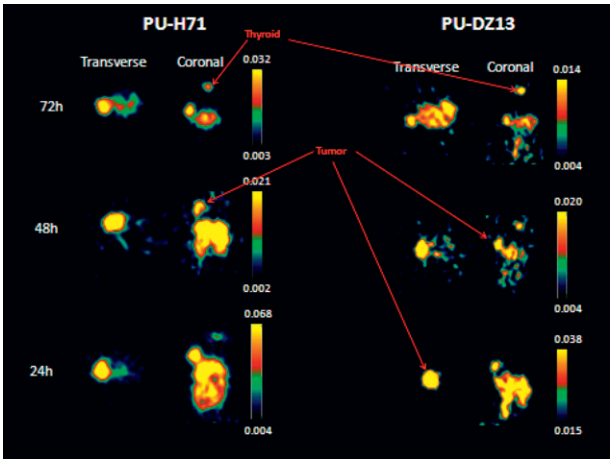

FIGURE 1.

*Travel award sponsored by the Society of Radiopharmaceutical Sciences.
**Travel award sponsored by the Academy of Molecular Imaging.

7**

Anatomical based development of breast phantoms for use with dedicated breast PET scanners. J. Saiz[1], S. Huang[1], J. Poon[1], A. Ferrero[1], R.D. Badawi[1]; 1. UC-Davis, Davis, CA

Objectives: Dedicated breast PET scanners have been intensively investigated in recent years as their improved sensitivity and resolution are hypothesized to result in improvements in the early detection and determination of treatment response for breast cancer. However, there is currently no well-defined protocol for accurately evaluating their performance. This work aims to determine parameters for a set of phantoms for estimating scatter and image quality in breast PET scanners. **Methods:** A collection of 216 dedicated pendant breast CT images were divided into quartiles of overall volume (v), radius closest to the chest wall (r), and total length of the breast (l). Using the quartile parameters for r and l, we determined the exponent in the equation of a half superellipsoid that matched each quartile v. We then defined a cylinder with the same v and the most overlapping volume as each half superellipsoid. These cylinders are our small, medium, and large breast phantoms, which will be made out of high density polyethylene. For each phantom, the line source will be placed with a radial offset of 4/5 of the phantom radius, as previous studies showed this to be the best location to estimate the scatter arising from a uniform, water-filled phantom of the same size. Out-of-field of view activity is modeled using the readily-available NEMA-NU2 2007 scatter phantom. Monte Carlo simulations using Geant4 Application for Tomographic Emission (GATE) will be performed to find the amount of activity to put in each line source in order to get the same true + scatter rates from dedicated breast PET scans of 3 patients. To determine the activity in the line source of the NEMA phantom, along with the calculated activity in each breast phantom, the singles rates will be matched to the same set of patient scans. **Results:** The parameters for each cylindrical phantom are as follows: small phantom – v = 442 mL, r = 4.8 cm, l = 6.1 cm; medium phantom – v = 680 mL, r = 5.3 cm, l = 7.7 cm; large phantom – v = 1040 mL, r = 6.1 cm, l = 8.9 cm. **Conclusions:** Based on dedicated breast CT images, we have geometrically determined parameters for a set of phantoms to be used in dedicated breast PET scanners in order to accurately measure scatter. Future work will focus on another set of phantoms to be used in dedicated breast PET scanners to measure image quality. These phantoms will have the same r and l dimensions as determined in this work.

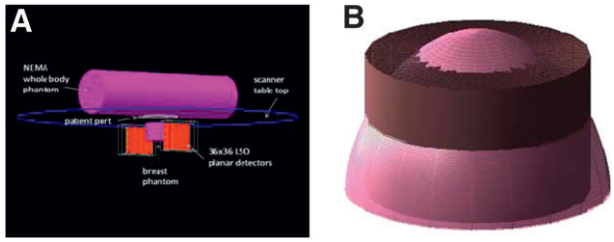

FIGURE 1. (A) GATE visualization of the phantom positions on the UC Davis breast PET scanner. (B) Overlay of the small breast phantom and its corresponding super-ellipsoid.

8*

PET imaging of the pre-metastatic niche in breast cancer animal models. M. Shokeen[1], A. Zheleznyak[1], J. Wilson[1], M. Jiang[1], K. Lam[2], J.K. Schwarz[1]; 1. Washington University School of Medicine, St. Louis, MO; 2. UC Davis Cancer Center, Sacramento, CA

Objectives: Recent studies have established a role for bone marrow-derived hematopoietic progenitor cells (HPCs) in the metastatic process. HPCs that express vascular endothelial factor receptor 1 (VEGFR1) and integrin α4β1 (also known as very late antigen 4 (VLA-4)) arrive at sites of metastasis and form a premetastatic niche/microenvironment. We aim to address an imaging strategy for in vivo imaging of HPCs at premetastatic sites before a secondary tumor is established. **Methods:** α4β1 negative MDA-MB-231/fluc human breast tumor cells were

implanted in nude mice through arterial circulation (left ventricle (l.v.)). Tumor cells spontaneously metastasized to distant sites including bone. The mice were monitored over a period of 30 days by a combined bioluminescence imaging (BLI)/microPET/CT imaging study to determine whether increases in PET signal with 64Cu-CB-TE2A-LLP2A, which has pM affinity for α4β1, was observed prior to tumors appearing in the bone. microPET images were acquired at 4 and 24 h after the administration of ca 200 μCi (7.4 MBq; SA: 19 MBq/nmol) of 64Cu-CB-TE2A-LLP2A. Standard uptake values (SUVs) of the bone were calculated from the microPET images using Amide and ASIPro. Simultaneous BLI was done to track the luciferase transfected tumor cells. **Results:** Two independent studies (n=7 and 8 mice, respectively) have suggested an influx of α4β1-positive HPCs prior to tumor cells homing to the site of metastasis. Cumulative SUV data from both experiments with mice imaged over a period of several days post l.v. tumor cell injection show an increased uptake of 64Cu-CB-TE2A-LLP2A ($p<0.05$) at the potentially metastatic bone sites (right and left legs). Figure 1 summarizes data from one of the studies showing cumulative SUV data (n=7 mice, 14 legs) with BLI/PET/CT images and histological validation of a representative mouse. The specificity of 64Cu-CB-TE2ALLP2A for α4β1 was validated in cell uptake studies. **Conclusions:** The presented data suggest feasibility of the premetastatic niche imaging by using the multimodality approach described herein.

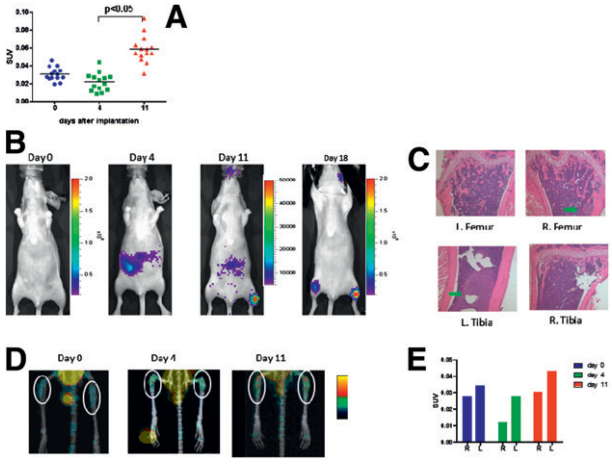

FIGURE 1. Up-regulation in radiopharmaceutical uptake occurs with and without visible tumor cell. (A) SUV uptake (cumulative; n=14) increases in bone over time. Representative Mouse (B-E): (B) BLI images over 0, 4, 11 and 18 days; (C) Corresponding histology (H&E staining) showing tumor present. Histology samples obtained at endpoint of experiment; (D) PET/CT images (days 0, 4 and 11) with focus on the leg bones; (E) (Right (R) and Left (L)) bone SUV uptake in the representative mouse.

9*

Synthesis and first in vivo evaluation of 18F-anti-HER2-Nanobodies: a new probe for PET imaging of HER2 expression in breast cancer. I. Vaneycken[1], C. Xavier[1], A. Blykers[1], N. Devoogdt[1], V. Caveliers[1], T. Lahoutte[1]; 1. In Vivo Cellular and Molecular Imaging, Vrije Universiteit Brussel, Brussels, Belgium

Objectives: Nanobodies (Nbs) are small (15kDa) antigen-binding fragments derived from heavy-chain antibodies that are naturally occurring in *Camelidae*. Nbs are attractive probes for molecular imaging because they bind a specific target extremely fast while unbound probes are rapidly cleared from the blood, resulting in high target-to-background ratios within the first hours after tracer injection. This pharmacokinetic profile is optimal for imaging with short-lived radio-isotopes such as 18F in combination with PET/CT or PET/MRI. In this paper we present the development of 18F-labeled Nanobodies for molecular imaging of HER2 expression in breast cancer patients. **Methods:** An anti-HER2 Nanobody was labeled with 18F using N-succinimidyl 4-[18F]fluorobenzoate ([18F]SFB) chemistry. [18F]SFB was synthesized as described before and incubated with 2rs15d at room temperature. Assessment of radiochemical purity and stability was performed using High Performance Chromatography (HPLC). Binding potential of the 18F-anti-HER2-Nb was evaluated in vitro using HER2-expressing SKOV-3 cells. Biodistribution and tumor targeting of the 18F-anti-HER2-Nb was evaluated in nude mice bearing HER2 positive LS174T xenografts. Additionally, blood clearance was analyzed in non-tumor bearing nu/nu mice. **Results:** After labeling, HPLC chromatograms showed a radiochemical purity >95%. The 18F-anti-HER2-Nb remained stable after 2,5h in PBS. *In vitro* studies showed that binding was specific with an affinity of 6.1 nM. *In vivo* biodistribution analysis showed that the 18F-anti-HER2-Nb was rapidly cleared from the blood via the kidneys with low retention in all other organs and tissues. The uptake in the HER2 positive tumor was 3.09±0.02 %IA/g, with a tumor-to-muscle ratio of 7.38±0.86 at 1 hour after intravenous injection. **Conclusions:** We showed for the first time the successful labeling of HER2 targeting nanobodies with 18F. The labeled probe retains nanomolar affinity for the HER2 receptor, and avid tumor uptake was demonstrated already at 1h post injection. 18F-anti-HER2-Nb PET imaging of breast cancer should enable non-invasive assessment of HER2 receptor status in breast cancer patients.

10**

Diffusion-weighted MRI as a possible biomarker of treatment response in a murine model of HER2+ breast cancer. J.G. Whisenant[1], L. Xu[1], J.C. Gore[1], T.E. Yankeelov[1]; 1. Vanderbilt University, Nashville, TN

Objectives: Diffusion-weighted MRI (DW-MRI) has been widely investigated in oncologic imaging; however, translation into routine clinical practice has been limited due to the lack of protocol standardization, inadequate understanding of whether changes in imaging parameters predict clinical outcomes related to therapy, and lack of validation for image interpretation. This study presents preliminary data on both the repeatability of DW-MRI, as well as its ability to assess treatment response in a murine model of HER2+ human breast cancer. **Methods:** Nude mice (n=9) with trastuzumab-resistant BT474 breast cancer xenografts were scanned with a respiratory-gated, diffusion-weighted spin echo sequence (*b* values=150, 500, 800 s/mm^2) on a Varian 7T. Apparent diffusion coefficient (ADC) maps were calculated via a monoexponential data fit, and mean ADC from the central tumor slice was compared between repeat acquisitions. Coefficient of variation (CV) and intraclass correlation coefficient (ICC) were calculated to evaluate repeatability. To investigate treatment response, 8 (4 control, 4 treated) additional nude mice injected with BT474 breast cancer cells were imaged with the same protocol as repeatability data at baseline, 24 and 48 hours after treatment (10mg/kg trastuzumab or drug vehicle), and 24 hours post second treatment. Average ADC from the central tumor slice was calculated at each time point. **Results:** CV and ICC were 13.3% ± 6.6% (mean±1.96*SE) and 0.88, respectively. ADC from a water phantom at a temperature of 32 °C was 0.0026 ± 0.0002 mm^2/s, which is within range of free water diffusion at 25 °C to 35 °C (2). Figure 1 displays parametric ADC maps of tumors from treated (a,b) and control (c,d) animals at baseline (left column) and Day 4 (right column). Average ADC at each time point is depicted in panels e and f for treatment and control groups, respectively. **Conclusions:** Repeatability results suggest a 13% change in ADC is required to observe effects from therapy rather than variations in imaging protocol. Preliminary investigation of ADC as a biomarker of response did show a difference between control and treatment groups; however, due to small sample size only a trend towards significance was observed (p=0.1). Nonetheless, this trend suggests that ADC could be used to assess response to trastuzumab. Ongoing studies include adding more animals in the longitudinal treatment study, as well as performing histology to correlate ADC with underlying biology.

*Travel award sponsored by the Society of Radiopharmaceutical Sciences.
**Travel award sponsored by the Academy of Molecular Imaging.

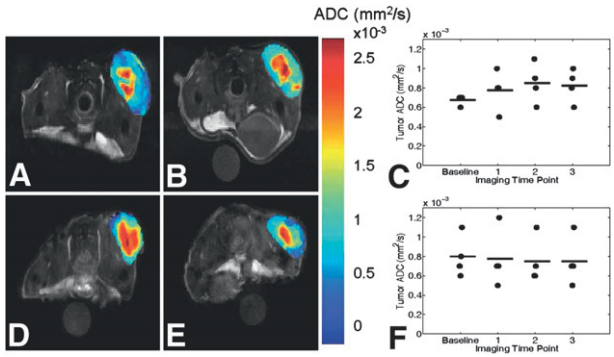

FIGURE 1. DW-MR images with corresponding tumor ADC parametric maps for a treated (a, b) and control animal (d, e) at baseline and Day 4. Panels c and f show average ADC as a function of treatment response for each mouse in both treatment and control groups, respectively. Note that after treatment, average ADC increases over time for the treatment group, whereas the ADC for the control group is relatively unchanged.

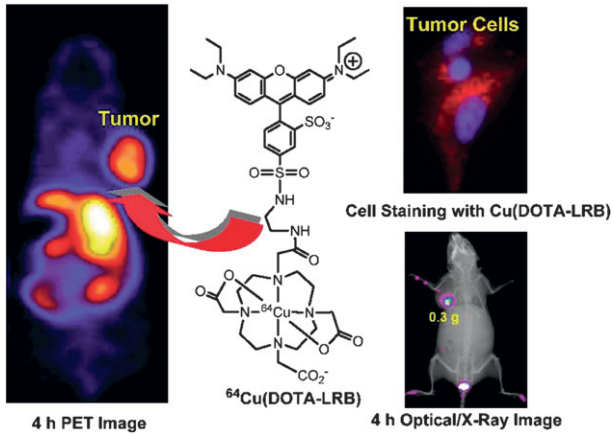

FIGURE 1. This report presents evaluations of 64Cu(DOTA-LRB) as a PET radiotracer and Cu(DOTA-LRB) as a fluorescent probe for tumor imaging in athymic nude mice bearing U87MG glioma and MDA-MB-435 breast cancer xenografts. The tumor is clearly seen at 4 h post-injection. The intracellular location of Cu(DOTA-LRB) is the energized mitochondria of tumor cells.

11*

Dual modality imaging of cancer with copper-labeled lissamine rhodamine B. Y. Zhou[1], X. Yan[1], Y. Kim[1], O. Jacobson[2], X. Chen[2]; 1. Purdue University, West Lafayette, IN; 2. National Institutes of Health (NIH), Bethesda, MD

Objectives: The enhanced mitochondrial potential in carcinoma cells is an important characteristic of cancer. It is of great current interest to develop a radiotracer that is sensitive to the mitochondrial potential changes at the early stage of tumor growth. In this report, we present the evaluation of 64Cu-labeled Lissamine Rhodamine B (LRB), 64Cu(DOTA-LRB), as a new PET (positron emission tomography) radiotracer and Cu(DOTA-LRB) as a fluorescent probe for tumor imaging in athymic nude mice bearing U87MG glioma and MDAMB-435 breast cancer xenografts. **Methods:** The athymic nude mice bearing U87MG human glioma and MDA-MB-435 breast cancer xenografts were used in the biodistribution, PET imaging and optical imaging studies. Both human tumor cell lines (U87MG and MDA-MB-435) and the cultured primary tumor cells (U87MG and MDA-MB-435) were used to explore the tumor localization mechanism. Normal human fibroblast cells were used as the control. Metabolism studies on 64Cu(DOTA-LRB) were performed using normal athymic nude mice. **Results:** 64Cu(DOTA-LRB) had high tumor uptake (6.54 ± 1.50, 6.91 ± 1.26, 5.68 ± 1.13, 7.58 ± 1.96, and 5.14 ± 1.50 %ID/g at 0.5, 1, 2, 4 and 24 h post-injection, respectively). The glioma tumors were clearly visualized as early as 30 min post-injection with 64Cu(DOTA-LRB) while the breast tumors were clearly visualized by optical imaging with Cu(DOTA-LRB). It was also found that 64Cu(DOTA-LRB) remained stable during renal excretion, but underwent extensive degradation during hepatobiliary excretion. Cellular staining studies suggested that Cu(DOTA-LRB) was able to localize in mitochondria of U87MG glioma and MDA-MB-435 breast cancer cells due to the enhanced negative mitochondrial potential as compared to that in normal cells of surrounding tissues. **Conclusions:** On the basis of the results from this study, it was concluded that 64Cu(DOTA-LRB) represents a new class of radiotracers for noninvasive imaging of glioma and breast tumors. Most importantly, Cu(DOTA-LRB) is also an excellent optical imaging agent, which makes dual modality imaging (PET and optical) possible using two probes (one is "hot" and the other is "cold"!) with the same chemical composition. In this way, one is able to demonstrate if the 64Cu radiotracer is able to selectively localize in tumors by PET, and at the same time one can visualize its intracellular location in tumor cells by optical imaging.

*Travel award sponsored by the Society of Radiopharmaceutical Sciences.

SECTION 2

12

Awareness, knowledge, and practices of breast cancer prevention among women with family history of breast cancer in first-degree relative in Ede Metropolis, Osun State, Nigeria. A. Adelekan[1]; 1. University of Ibadan College of Medicine

Objectives: This study was designed to assess knowledge and prevention practices among women with family history (FH) of the BRCA gene in the study area. **Methods:** This cross-sectional study was conducted in the 2 local government areas in Ede. Snowball sampling technique was used to select 187 women with FH of BRCA. A semistructured questionnaire was used to obtained data from the respondents. Knowledge of BRCA was assessed on a 20-point scale. A correct answer attracted a score of 2 points, while the score for a wrong answer was zero. Total scores less than 11 points or 11 points and above were considered poor and good knowledge, respectively. Descriptive statistics and t-test were used to analyze the data. **Results:** The mean age of the respondents was 35.5±7.1 years. The majority (81.9%) were married. More than half (57.8%) have no education. Many (65%) were not aware of their susceptibility to BRCA. Most (97.4%) of respondents have family members who had died of BRCA, and 73.2% have family members who currently have BRCA. Respondents' mean knowledge score was 9.2±3.1. Respondents mostly believed causes of BRCA were spiritual powers (57.9%) and oral contraceptive pill (54.9%.). Some (35.7%) of respondents do not know cancer can be cured if detected early, and high proportion (78.5%) do not know how breast self-examination (BSE) is done. The educational level of the respondents positively influenced their knowledge ($P<0.05$). The prevalence of alcohol consumption, physical inactivity, early menarche (age < 11 years), and nulliparity were 7.2%, 58.7%, 42.8% and 30.7% respectively. Preventive practices among respondents included breastfeeding for longer than 1 year (70.5%), regular exercise (13.6%), and weight loss (10.9%). Almost all (97.9%) and 57.5% have never undergone mammography or BSE respectively. Perceived barriers included fear of discovering abnormality (82.7%) and lack of access to mammography (98.3%). **Conclusions:** Knowledge of breast cancer was low, and incorrect preventive practices exist among respondents. Information, education, and communication program on breast cancer prevention should be intensified for these women.

13

Effectiveness of training on knowledge, perceptions, and self-efficacy of breast self-examination among women with family history of breast cancer in Ede, Osun-State, Nigeria. A. Adelekan[1]; 1. University of Ibadan College of Medicine

Objectives: The study assessed women with family history of BRCA gene for their knowledge, perceptions, and self-efficacy in relation to BSE practices in Ede, Nigeria. **Methods:** The quasi-experimental study involved an experimental group of 20 women selected in Ede and a control of 30 women in Ara. The 2 groups completed a pretest using a validated questionnaire, and the results were used for designing a 4-day training intervention for the experimental group. A post-test was conducted among the 2 groups using the same questionnaire. Data were analyzed using descriptive, Chi-square, and t-test statistics. **Results:** The mean ages of the experimental and control groups were 35.8 ± 5.2 and 36.1 ± 5.3 years respectively. The experimental and control groups' mean knowledge scores at pretest using a 50-point knowledge scale were 15.2 ± 12.3 and 17.5 ± 10.2 respectively. Mean scores at post-test for the experimental and control groups were 46.9 ± 2.1 and 19.3 ± 15.2 respectively ($P<0.05$). A significant difference was found between the experimental group's pretest (15.2 ± 12.3) and post-test (46.9 ± 2.1) scores ($P<0.05$). The control's mean pretest and post-test knowledge scores of 17.5 ± 10.2 and 19.3 ± 15.2 respectively were not significantly different. At pretest, none of the respondents in either the experimental or control group knew the risk factors of BRCA; at post-test all (100%) participants in the experimental group and none in control group could state these risk factors. Perception of the experimental group that BRCA is mostly caused by spiritual powers changed from 85.9% at pretest to 3.1% at posttest ($P<0.05$), while for the control perceptions were 88.5% and 85.7% for pretest and post-test respectively, with no significant difference. The perception that BRCA cannot be cured if detected early changed from 75.6% at pretest to 1.3% at post-test among the experimental group; among the control, the proportions of participants with this perception at pretest and post-test were 83.2% and 79.9% respectively. In the experimental group, participants' self-efficacy relating to practices of BSE rose significantly from 13.2% to 100% at post-test ($P<0.05$); the values among the control at pretest and posttest were 14.2% and 13.9% respectively with no significant difference. **Conclusions:** Training intervention was effective in improving women's knowledge and influenced their perception and self-efficacy relating to the prevention of breast cancer.

14

Near-infrared imaging of breast cancer-related lymphedema. M.B. Aldrich[1], C. Flfe[2], J. Rasmussen[1], I.C. Tan[1], M.V. Marshall[1], E.M. Sevick-Muraca[1]; 1. Center for Molecular Imaging, IMM, UTHealth, Houston, TX; 2. Memorial Hermann Hospital, Houston, TX

Objectives: To assess lymphatic vessel architecture and pumping anomalies in breast cancer–related lymphedema (BCRL) and normal control subjects as a function of time since BCRL onset. **Methods:** We used near-infrared (NIR) imaging to observe lymphatic vessel architecture and pumping function in BCRL and normal control subjects. **Results:** We found increasing severity of lymphatic vessel anomalies with increased time since lymphedema onset. This study is the first temporal assessment of BCRL development after cancer treatment. **Conclusions:** NIR imaging provides exquisite images and movies of lymphatics, and the technology could be used for cancer and lymphedema diagnosis, detection of cancerous lymph nodes, and assessment of therapeutics. Our findings suggest causes of BCRL and provide impetus to encourage early, aggressive detection and treatment of this debilitating disorder.

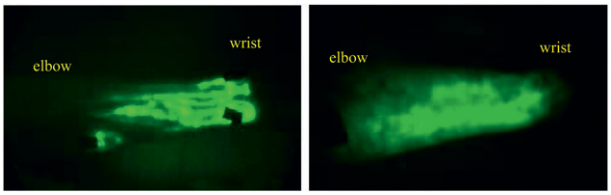

FIGURE 1. Normal (left) and breast cancer-related lymphedema (right) near-infrared lymphatic images of forearm undersides.

15

Molecular breast imaging with CZT detectors: initial experience at the Tel Aviv Sourasky Medical Center. I.M. Blevis[1], E. Even-Sapir[1]; 1. General Electric Healthcare, Haifa, Israel

Objectives: Molecular breast imaging (MBI) for the detection of breast cancer has recently become of interest because of the development of high-resolution and adaptable compact gamma cameras (from the semiconductor CZT). Because of the characteristics of gamma imaging, image quality is sustained for all breast tissue including dense breast tissue. Patient acceptance is expected to be high because there is no need to compress the breast to improve image quality or ease of reading. Clinical trials have begun at a few institutions. The objective of this study is to summarize initial experience with a dual-headed MBI camera (Discovery 750b, GE Healthcare, Haifa, Israel) at the Tel Aviv Sourasky Medical Center. **Methods:** Patients referred for diagnostic imaging were injected with 740MBq Tc-sestamibi and then imaged with a dual-head MBI camera. The studies consisted of 2 views from the 2 detectors (upper and lower) and an arithmetic average image for both CC and MLO acquisitions of 10 minutes each. Reviewing physicians graded the images as 1= probably benign, need no further investigation (FI); 2= equivocal, needs FI; and 3, highly suspicious for disease. Currently 55 patients have been imaged. The different indications were: unclear lesions on mammography or ultrasonography where the patient was too big or had a contraindication for MRI; for disease staging prior to neo-adjuvant therapy; assessment of treatment response post neo-adjuvant therapy; unclear detected lesions postlumpectomy; BRCA patients with very dense breast tissue; and searching for the primary lesion in women who were diagnosed with axillary node metastasis. **Results:** Analysis results for 24 patients are completed. MBI detected 14 known cancers and missed one. It also identified unexpected malignant lesions in the contra-lateral breast in 2 patients. MBI ruled out active disease in 6 patients and was false positive in 3, detecting increased uptake in benign lesions (fibroadenoma, postsurgical changes, and sclerosing adenosis). **Conclusions:** These initial findings on the use of a novel scintimammography device composed of new generation of CZT detectors are encouraging. Further investigation is indicated in order to define the role of MBI in the imaging algorithm of the breast in various patient groups.

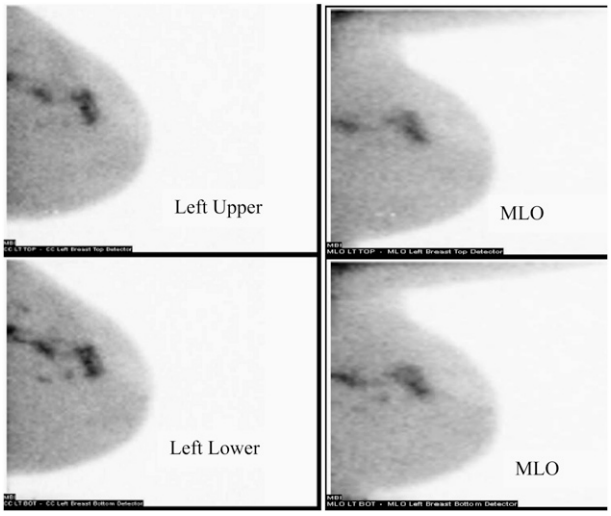

FIGURE 1. A 73-year-old female patient with bifocal lesions detected on mammography in the left breast. These lesions were found on biopsy to be infiltrative ductal carcinoma. On MBI of this breast, multiple lesions accumulating 99mTc-MIBI were suggestive of multifocal, multicentric disease. Based on these findings, the patient underwent MRI, which validated the extent of the disease. The patient was referred for neoadjuvant chemotherapy.

16

Pilot study of freehand SPECT for sentinel lymph node biopsy in breast cancer patients. C. Bluemel[1], A. Ehlerding[2], A. Okur[1], T. Wendler[3], A. Schnelzer[2], K. Scheidhauer[1]; 1. Department of Nuclear Medicine, Klinikum rechts der Isar, Technische Universitaet Muenchen, Munich, Germany; 2.

Department of Gynecology, Klinikum rechts der Isar, Technische Universitaet Muenchen, Munich, Germany; 3. Surgiceye GmbH

Objectives: Evaluation of performance of sentinel lymph node biopsy in breast cancer patients using innovative freehand SPECT (fhSPECT). **Methods:** To date, 32 breast cancer patients (37–84y) undergoing sentinel lymph node (SLN) biopsy were recruited and scanned intraoperatively using fhSPECT (declipseSPECT by SurgicEye, Munich, Germany). Protocol consisted of counting the number of SLNs detected with both gamma probe (GP) and fhSPECT before incision and comparing these results with planar scintigraphy (PS) acquired the day before. After excision and control of basin using GP, fhSPECT images were used to verify absence of radioactivity. Additionally detected hot spots by fhSPECT were confirmed with GP and if clinically indicated resected by surgeon. **Results:** Preoperatively, 61 SLNs were mapped with conventional PS (54-127MBq). In the preincision scan, fhSPECT managed to map all but 3 SLNs in the identical position as compared to node location at PS, as well as 1 further SLN. GP mapped in total 46 of 61 nodes (30/32 pts). Both fhSPECT and GP failed to detect any SLNs in 1 patient during preincision scan due to extremely low uptake. In total 53 SLNs were resected and confirmed to be radioactive ex-vivo. Metastatic involvement was found 3 of these SLNs. fhSPECT detected 11 SLNs (11 pts) postexcision despite initial free measurement with GP, whereof 6 were resected. However, the protocol used did not allow determination of whether the additionally resected nodes changed the final pathological nodal status. In the remaining 5 patients where fhSPECT detected additional nodes, harvesting of these nodes was discarded, as higher-uptake SLNs had been removed already. The surgical procedure was extended in total by approx. 5 min. **Conclusions:** Preliminary experience indicates that intraoperative imaging with fhSPECT for lymphatic mapping enables more intuitive and more sensitive detection of SLNs preincision than the use of GP alone (95% vs. 75%, assuming PS as ground truth). fhSPECT showed additional radioactive nodes in 34% of patients and motivated additional harvest of SLNs in 19% (6/32 pts). Despite the fact that no change in therapy could be proven in this study, the number of additional SLNs found by fhSPECT suggest setup of a bigger prospective study to clarify the impact of fhSPECT on the pathological nodal status, therapy, and probably prognosis. Alteration of the surgical workflow was considered minimal given potential clinical advantages, like assurance of complete resection and minimized invasiveness.

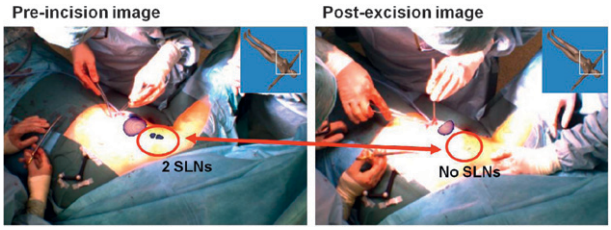

FIGURE 1.

17

A clinical evaluation of breast tissue uptake of Tc99m-sestamibi as a function of injected dose. M. Böhm-Vélez[1], D. Kieper[2], M.B. Williams[3], T.S. Chang[1], B.H. Ward[1], M.R. Straka[1]; 1. Weinstein Imaging Associates, Pittsburgh, PA; 2. Department of Physics, Hampton University, Hampton, VA; 3. University of Virginia, Charlottesville, VA

Objectives: The Tc99m-Sestamibi drug package insert recommends 740–1110 MBq for breast imaging; however, this dose was established using standard gamma cameras. There are now several breast-optimized gamma cameras available with up to 4 times higher photon sensitivity. This study is designed to investigate if there are physiologic limitations to reducing the dose by comparing breast tissue uptake of sestamibi at a standard 740 MBq dose to that at lower doses. **Methods:** Patients routinely scheduled for breast scintigraphy were imaged using a Dilon 6800 gamma camera following the SNM Practice Guidelines for Breast Scintigraphy (2010). Each had a standard 740 MBq dose separated into 2 syringes containing either two 370 MBq doses or a 185 and a 555 MBq dose. Each syringe activity was measured immediately prior to injection. Thirty-two subjects were randomized into receiving fractional doses of 185 (n=11), 370 (n=10), or 555 (n=11) MBq followed by bilateral CC acquisitions. Then the remaining fraction of the 740 MBq dose was delivered, and a normal 4-view imaging procedure was conducted. A region of interest encompassing the breast was drawn in each CC image, and the average number of counts per pixel (ACP) was calculated. Following correction of the ACP values for radioisotope decay and biological washout (described by Del Vecchio et al, J Nucl Med 1997; 38:1348-51), the ACP of the first (low-dose) image was expressed as a percentage of the ACP of the 740 Mbq image for each breast. The left and right breast percentages were averaged and compared to the activity of the first injected dose expressed as a percentage of the total injected dose. **Results:** For first injected doses of 185 MBq, 370 MBq, and 555 MBq, the difference between the injected dose ratio and the measured uptake ratio was 0.04%, 1.3%, and 5.9%, respectively. Given the null hypothesis of equal ratios, the 2-tailed t test p values for these differences were 0.98, 0.60, and 0.08, respectively. **Conclusions:** These preliminary results suggest the uptake of sestamibi in breast tissue may not be proportional to the injected dose, with decreased proportionality for higher injected doses. It is not yet understood why this nonlinearity exists or if it impacts the efficacy of breast scintigraphy at lower doses. More work is needed to determine if imaging at lower doses impacts the contrast of breast lesions.

18

A new 64Cu-labeled cyclic peptide for microPET imaging of interleukin 11 receptor alpha-chain in a breast cancer model. K. Chen[1], L. Yap[1], R. Park[1], P.S. Conti[1]; 1. University of Southern California, Los Angeles, CA

Objectives: Experimental evidence has shown that interleukin 11 (IL-11) and its receptor alpha-chain (IL-11Rα) are associated with breast cancer development and progression and may play a vital role in the bone metastasis of human breast cancer. The aim of this study is to synthesize and evaluate a new 64Cu-labeled cyclic peptide for microPET imaging of IL-11Rα in a breast cancer model. **Methods:** The cyclic peptide [c(CGRRAGGSC)], named ILP, was conjugated with the macrocyclic chelating agent 1,4,7,10-tetraazadodecane-N,N',N'',N'''-tetraacetic acid (DOTA) in the presence of N-hydroxysulfosuccinimide (Sulfo-NHS), N-(3-dimethylaminopropyl)-N'-ethylcarbodiimide (EDC) and N,N-diisopropylethylamine (DIPEA). The resulting DOTA-ILP conjugate was confirmed by mass spectrometry (MS) analysis and labeled with 64Cu in ammonium acetate buffer. Small animal PET imaging studies were carried out in female athymic nude mice bearing subcutaneous MDA-MB-231 xenografts. **Results:** The DOTA-ILP was synthesized in 85% yield. 64Cu labeling was achieved in 80 to 90% decay-corrected yield with radiochemical purity of >98%. The specific activity of 64Cu-DOTA-ILP was estimated to be ~37 MBq/nmol. No significant difference between 64Cu-radiolabeled tracer and unlabeled conjugate was observed by analytical HPLC. The 64Cu-DOTA-ILP tracer demonstrated high hydrophilicity, as determined by octanol–water partition coefficient measurements, with a log P value of −2.28±0.03. PET imaging results showed that 64Cu-DOTA-ILP has preferential tumor uptake in MDA-MB-231 xenografts with reasonable tumor washout (4.37±0.95 %ID/g at 24 h after injection). The biodistribution results were consistent with the quantification analyses of microPET imaging.

19

Molecular imaging with FDG PET-CT is the current choice for response evaluation of bone metastasis in breast cancer?

M. Gupta[1], P.S. Chaudhary[1], A.K. Chaturvedi[1], P. Sharma[1]; 1. Rajiv Gandhi Cancer Institute & Research Centre, New Delhi, India

Objectives: Current results show promising role of FDG PET CT in response evaluation for bone metastasis in carcinoma breast. A 50% cutoff for SUVmax for partial response and absence or normalization to contra lateral/adjacent normal bone as complete response appear to be appropriate criteria. Final impact on progression-free survival needs longer follow-up. Accuracy in diagnosis and response is important to ensure effective palliation, longer progression-free survival, and improved quality of life. With conventional imaging response, evaluation for bone metastasis is difficult, which shows persistent changes on CT or tracer uptake on bone scan. Presently RECIST 1.1 is the standard available criteria for response evaluation of lytic lesions in

clinical research. MD Anderson (MDA) criteria dedicated to bone metastasis are also based on conventional imaging, subjective in nature, and not very well-known. Our objective was to evaluate where FDG PET CT is the current imaging modality of choice for response evaluation for bone metastasis in breast cancer and, if yes, identify the appropriate response criteria. **Methods:** Twenty-nine women with carcinoma breast and bone metastasis without previous treatment for bone metastasis were included in the analysis. Each patient had at least baseline and interim FDG PET CT scans (post 3 or 4 cycles of chemotherapy). Standard whole-body PET-CT acquisition protocol was followed. Standardized uptake value normalized to body weight (SUVmaxBW) was used for response evaluation. Standard RECIST criteria were used for evaluation of CT, and at least 50% fall in SUV max on a lesion-by-lesion basis was interpreted as PR on PET and absence of metabolic activity or equal to adjacent/contralateral normal bone as CR. **Results:** Fifteen of 29 patients had bone metastasis at primary presentation, while 14/29 patients had bone metastasis after primary breast cancer treatment. Twenty-six patients had 2 or more sites of bone involvement. Eight of 29 patients had only bone limited metastasis. Nine of 29 (31%) of patients' interim evaluations showed discordant results on metabolic and morphologic imaging. Eight patients had complete response based on PET, compared to 2 by CT alone. Sixteen of 29 patients were on hormonal treatment for metastasis and expected to have either stable disease or partial response, but in spite of 50% cutoff (30% for RECIST 1.1), PET showed better results. All patients with CR on only PET were in remission, with avg. 10-month follow-up. **Conclusions:** Current results show promising role of FDG PET CT in response evaluation for bone metastasis in carcinoma breast. A 50% cut off for SUVmax for partial response and absence or normalization to contra lateral/adjacent normal bone as complete response appear to be appropriate criteria. Final impact on progression-free survival needs longer follow-up.

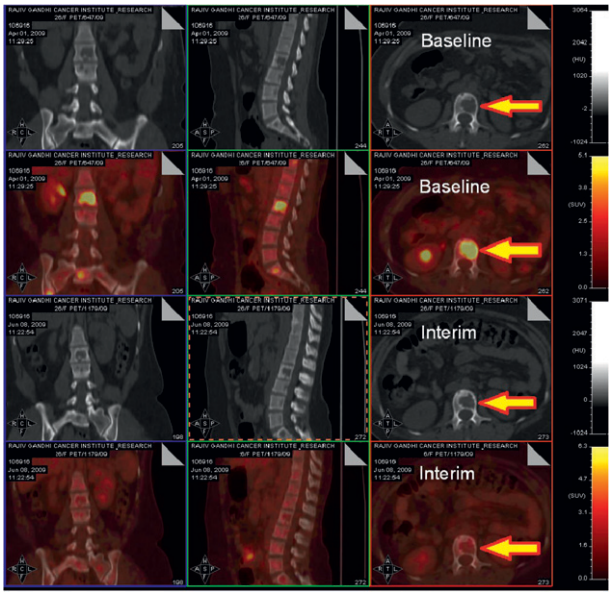

FIGURE 1.

20

Variation in Tc-99m sestamibi background parenchymal uptake with menstrual cycle in premenopausal women undergoing molecular breast imaging. C.B. Hruska[1], D.J. Rhodes[1], D.A. Collins[1], M.K. O'Connor[1]; 1. Mayo Clinic, Rochester, MN

Objectives: In the Mayo Clinic experience of performing Molecular Breast Imaging (MBI) with Tc-99m sestamibi, we have occasionally observed patterns of background parenchymal uptake (BPU) of radiotracer which appears to be affected by menstrual cycle. The goal of this study was to evaluate the effects of menstrual cycle phase on MBI. **Methods:** MBI was performed in premenopausal volunteers who had negative recent mammogram, had regular menstrual cycles, and were not currently using hormonal contraceptives or hormonal drugs such as estrogen/progesterone therapy, SERMs or aromatase inhibitors. Each participant underwent two MBI studies, timed from the start of menstrual cycle; MBI was performed during follicular phase (within days 5-10) and during luteal phase (within days 20-25). MBI was performed with dual-head cadmium zinc telluride detectors. For each MBI study, participants received 10 mCi Tc-99m sestamibi, and mediolateral oblique views of each breast were obtained for 10 minutes per view. A radiologist categorized the pattern of BPU on MBI as either photopenic, minimal-mild, or moderate-marked and subjectively assessed changes in BPU between the two phases. Mammographic density was also subjectively assessed for each subject. **Results:** A total of 44 premenopausal women were studied. Median age was 41 (range 35-45). Mammographic density was <25% in 4, 25-50% in 14, 50-75% in 22 and >75% in 4. In 17/44 (39%) women, moderate-marked BPU was not observed in either phase (categorized as photopenic or minimal-mild). Moderate-marked BPU was present on luteal phase MBI only in 10/44 (23%) women and on follicular phase MBI only in 1/44 (2%) women. In 7/44 (16%) women, moderate-marked BPU was present on follicular phase MBI and increased in luteal phase MBI, and in 9/44 (20%), moderate-marked BPU was present on MBIs at both phases and unchanged. In all cases, areas of BPU spatially correlated with areas of mammographic density. The presence of moderate-marked BPU occurred in all density categories but was more likely to occur in women with >50% density compared to women with <50% density. **Conclusions:** Patterns of moderate to marked background parenchymal uptake were observed in ~60% of premenopausal women studied and were more likely to occur during luteal phase, suggesting that MBI should be performed during follicular phase for best diagnostic quality. These findings indicate that Tc-99m sestamibi in breast tissue is related to exogenous hormone levels which fluctuate during the menstrual cycle.

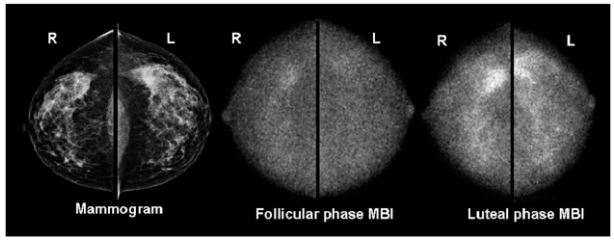

FIGURE 1. The mammogram and MBI images from follicular and luteal phase imaging times of a patient with mammographic density between 50-75% dense. Uptake is substantially increased during the luteal phase.

21

Multiparametric MRI reveals early response patterns to antiangiogenic therapy in primary breast cancer. N.P. Hughes[1], S. Mehta[2], R.F. Adams[3], S.S. Gambhir[4], A.R. Padhani[5], A.L. Harris[2]; 1. Stanford University School of Medicine, Stanford, CA; 2. University of Oxford, Oxford, UK; 3. Oxford Breast Imaging Centre, Churchill Hospital, Oxford, UK; 4. Stanford University, Stanford, CA; 5. Paul Strickland Scanner Centre, Mount Vernon Hospital, London, UK

Objectives: Despite the widespread use of antiangiogenic drugs to treat cancer patients, there is currently little understanding of which patients benefit most from this type of therapy. The objective of our study was to assess the use of multiparametric magnetic resonance imaging (MRI) to identify the early patterns of response to bevacizumab therapy in primary breast cancer. **Methods:** We designed a window-of-opportunity study in which bevacizumab is administered as a short-term first-line treatment to primary breast cancer patients. Multiparametric MRI scans, core biopsies for gene expression analysis, and blood samples for proteomics were performed immediately before and 2 w after bevacizumab therapy. Our imaging protocol was designed to interrogate multiple aspects of the tumor microenvironment. In particular, we performed diffusion-weighted imaging (DWI) to assess tumor cellularity, blood oxygen level–dependent (BOLD) imaging to assess

the oxygenation status of red blood cells in perfused regions of the tumor, and finally dynamic contrast-enhanced (DCE) MRI to assess the tumor vasculature. The DWI and BOLD sequence data were used to generate parametric maps of the apparent diffusion coefficient (ADC) and the apparent transverse relaxation rate (R2*), respectively. For the DCE-MRI analysis, we used pharmacokinetic modeling (specifically Tofts' model with a population-based input function) to quantify the volume transfer constant Ktrans on a voxel-wise basis. **Results:** We enrolled 47 patients with primary breast cancer and analyzed the imaging data for 44 patients with good-quality MRI scans. Our analysis revealed 3 key patterns of response to bevacizumab. The first pattern (77% of patients) is associated with a vascular response, reflected in a decrease in Ktrans values across the tumor. The second pattern (5%) is associated with the development of a large central necrotic core, as evidenced by a significant increase in the ADC values, together with a dramatic reduction in vessel permeability and blood flow as measured by Ktrans. The third pattern (18%) shows either no change in any of the imaging parameters or an increase in the Ktrans values over the 2 weeks of therapy. **Conclusions:** Multiparametric MRI revealed 3 different patterns of early response to bevacizumab therapy in primary breast cancer. Knowledge of these early response patterns, and the associated changes in tumor biology, may aid in patient selection for anti-angiogenic therapy and ultimately lead to improved cost-effectiveness for these drugs.

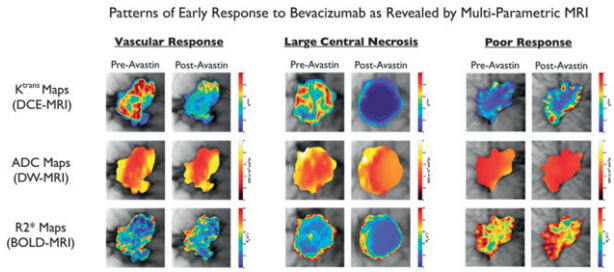

FIGURE 1. Patterns of early response to bevacizumab as revealed by multiparametric MRI

22

Positron emission mammography (PEM) measures of FDG uptake at 3 postinjection time points. L. MacDonald[1], J. Rogers[2], J.D. Beatty[2]; 1. University of Washington Radiology, Seattle, WA; 2. Swedish Cancer Institute, Seattle, WA

Objectives: To investigate lower dose in positron emission mammography (PEM), we scanned patients at 3 time points to observe image quality at later times in which activity is reduced by decay. Image noise is affected by injected dose and uptake time. An additional consideration in observing later images is that relative tracer uptake has been seen to increase with time-after-injection in certain lesions. The objective of this work was to study 18-F fluorodeoxyglucose (FDG) uptake in breast tissue as a function of postinjection time using PEM scanning. **Methods:** Confirmed breast cancer patients underwent FDG-PEM scanning prior to treatment; 203±7.6 MBq FDG was injected, followed by single-view 14-min PEM scans at 60, 90, and 120 min postinjection (PEM Flex Solo II). Regions of interest (ROIs) were drawn around lesions, and in 2 background (BG) areas free of abnormalities on each image; BG ROIs contained adipose, glandular, or mixed tissue. Due to lack of quantitative corrections on the PEM Flex scanner, FDG uptake in lesions was calculated relative to BG as lesion:background ratio (LBR) = (lesion-max)/(BG-mean). **Results:** In 8 patients analyzed thus far, there were 10 malignant lesions identified (3.6-30mm, mean=13mm): 5 infiltrating ductal carcinoma (IDC), 2 infiltrating lobular carcinoma (ILC), 2 ductal carcinoma in situ (DCIS), and 1 mixed-pathology site (IDC+DCIS). Mean LBR change between 60-min and 120-min postinjection scans was: IDC: 55±23% (range 32−81%, P<0.01); ILC: 13% (−9.9 to +36%); DCIS: 5.4% (5.3−5.5%); mixed: 9.6%, where values >0 reflect an increase. Decay-corrected mean background decreased 16±12% (range: −39% to +9.8%, P<0.01). Coefficient of variation in BG ROIs increased 18±20% (−24% to +55%, P<0.01). **Conclusions:** PEM LBR in IDC increased between 60 and 120 min postinjection. BG uptake decreased, but our results did not distinguished adipose and glandular tissues known to exhibit different FDG uptake, and results have not been corrected for patient mass, an important factor in absolute BG. A standard is needed in placing BG ROI for LBR calculations. While no loss of image features was observed due to lower activity on 120 min postinjection scans, LBR tended to be higher, so lower dose at earlier time, with the associated lower LBR, needs evaluation for contrast-to-noise properties. Other detector metrics (e.g. dead time) also need consideration.

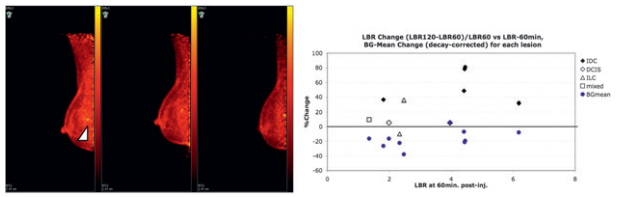

FIGURE 1. Positron emission mammography (PEM) measures of FDG uptake at 3 postinjection time points: 60, 90, 120 min postinjection. (A) RMLO, 3.6 mm IDC (LBR=1.8 at 60min). Lesion (arrow) is separated from the edge artifacts on the 60- and 90-minute postinjection images, but at 120 min, placement of the breast in the scanner resulted in the lesion being on the edge of the image and within the region of high-variance edge artifacts. (B) Change in LBR vs. LBR on the 60-min post-injection images. Solid circles are the change in BG-mean corresponding to each lesion.

23

Diagnostic imaging for breast cancer detection via 3D multimodal ultrasonic tomography. V.Z. Marmarelis[1], M. Sofras[2], S. Hadjuagapis[2], D. Koulocheri[3], P. Liakou[4], G. Zografos[4]; 1. University of Southern California Biomedical Engineering Department, Los Angeles, CA; 2. MastoScopia S.A., Athens, Greece; 3. Hippokration University Hospital, Athens, Greece; 4. University of Athens, School of Medicine, Athens, Greece

Objectives: To demonstrate the potential capabilities of a new 3D diagnostic imaging technology, termed *multimodal ultrasonic tomography (MUT),* for early detection of breast cancer via initial clinical trials in the EU. **Methods:** We performed 3D tomographic scans of pendulant breasts in water-bath for 54 volunteers (after informed consent) using transmission ultrasound in a fixed-coordinate system for multiple view-angles and scanning planes. Specially coded sequences of broadband ultrasonic pulses were used and properly analyzed with novel methodologies to obtain MUT images of refractivity, frequency-dependent attenuation, phase-velocity, and dispersion. In-plane pixel size was 0.25 mm × 0.25 mm and vertical separation between adjacent coronal slices was 2–4 mm (depending on clinical requirements). These MUT images provide "classification vectors" at each tissue voxel that can be used for tissue characterization/differentiation in each coronal slice. The hypothesis that this multimodal information can be used for reliable detection and differentiation of breast lesions was examined with MUT data from 54 female volunteers with median age of 57 years and BI-RADS 4 mammogram diagnosis, presenting 89 lesions (41 malignant and 48 benign). All lesions were confirmed via pathology of biopsy samples or mastectomy specimens obtained in the normal course of clinical practice. There were no operational complications in any of the MUT scans, and all volunteers attested to total comfort. **Results:** All 89 lesions were clearly detected on the MUT diagnostic images and also classified correctly into benign (48) or malignant (41) using their respective multimodal information. An illustrative example of composite MUT "diagnostic images" is shown in Figure 1, depicting a large benign and a small (6 mm × 4 mm) malignant lesion. The calibrated scoring values of the composite MUT "diagnostic images" (based on the aforementioned physical attributes) were found to cluster in a manner that allows reliable delineation between malignant lesions, benign lesions, and normal tissues. Malignant lesions generally exhibited higher values of refractivity, attenuation, and dispersion. **Conclusions:** Initial clinical results have demonstrated the ability of the MUT technology to detect all 89 BIRADS 4 lesions discernible in mammograms of 54 volunteers and, furthermore, confirmed the automated lesion differentiation capability of MUT utilizing multimodal ultrasonic information.

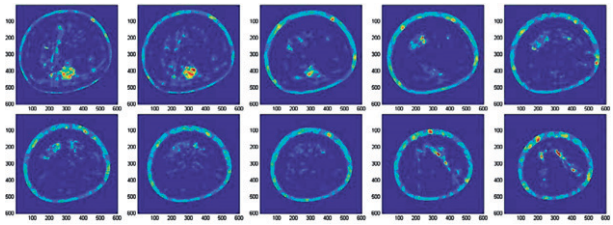

FIGURE 1. Illustrative example of 10 coronal slices of the composite MUT "diagnostic image" (Volunteer #037) depicting a large benign lesion on slices 01–03 and a small malignant lesion (6 mm × 4 mm) on slices 09–10. The field of view is 150 mm, the in-plane pixel size is 0.25 mm × 0.25 mm, and the inter-slice distance is 4 mm.

24

Low-dose molecular breast imaging. M.K. O'Connor[1], C.B. Hruska[1], D.J. Rhodes[1], A.L. Weinmann[1], C.L. Tortorelli[1], R. Maxwell[1], A.L. Conners[1]; 1. Mayo Clinic, Rochester, MN

Objectives: The aim of this study was to achieve a 5-fold reduction in the necessary dose of Tc-99m sestamibi to perform molecular breast imaging (MBI). **Methods:** Two MBI detectors are under study at our institution: LumaGem (Gamma-Medica Ideas [GMI], Northridge, CA) and Alcyone (General Electric [GE] Medical Systems, Haifa, Israel). Both systems comprise dual-head pixilated CZT detectors mounted on a modified mammographic gantry. The dual-head design was previously shown to significantly increase detection of small breast lesions compared to a single head design. The following 3 dose reduction methods were employed. (1) Low-dose collimation: Optimized registered collimators were designed for each gamma camera in order to improve system sensitivity while retaining adequate spatial resolution. For both designs, hole length was shortened and septal thickness increased from standard collimation. (2) Energy acceptance window: The standard energy window used with Tc-99m sestamibi is typically 126 – 154 keV. From Monte Carlo modeling of patient energy spectra, we determined that a lower energy window limit of 110 keV would capture a substantial proportion of misregistered photopeak events while including only a small amount of scattered events into the image. (3) Postprocessing filters: Noise reduction algorithms were developed to generate 4 composite images (one from each CC and MLO view of each breast). A Gaussian neighborhood geometric mean (GNGM) was used to adaptively combine opposing images in order to decrease noise but retain lesion contrast. A non–local-means denoising filter was applied to the combined images. The impact of these dose reduction methods was evaluated in phantom and patient studies. **Results:** Optimized collimation and widened energy window resulted in a gain in sensitivity of 3.6 for the LumaGem and 2.8 for the Alcyone detectors. With application of all 3 dose-reduction methods, 148 MBq images had slightly fewer counts but comparable or improved signal-to-noise ratio (SNR) compared to the standard 740 MBq images. Clinical low-dose MBI studies showed comparable quality to previous standard studies and in 3 studies, mammographically occult breast cancers were detected with low-dose MBI. **Conclusions:** Image quality obtained with low-dose MBI performed with 148 MBq Tc-99m sestamibi matches that of standard MBI performed with 740 MBq dose. Low-dose MBI presents radiation risks to the patient comparable to that of digital screening mammography, allowing its safe implementation as a screening technique.

25

Molecular breast imaging (MBI) in the preoperative evaluation of women with biopsy-proven breast cancer. M.K. O'Connor[1], C.B. Hruska[1], D.J. Rhodes[1], A.L. Conners[1], C.L. Tortorelli[1], R. Maxwell[1], J.C. Boughey[1]; 1. Mayo Clinic, Rochester, MN

Objectives: The aims of this study were to determine whether MBI is more sensitive than mammography (a) in detecting additional foci of breast cancer in the ipsilateral breast, (b) in detecting additional foci of breast cancer in the contralateral breast, and (c) in the evaluation of disease extent of biopsy-proven disease. **Methods:** Patients with biopsy-proven breast cancer scheduled for surgery were offered enrollment in this study. All patients had a diagnostic mammogram and an MBI study prior to surgery. Patients with MBI studies showing additional sites of disease underwent additional diagnostic studies. At the time of operation the pathologic findings were correlated with the MBI results. MBI studies were performed using a LumaGem system (Gamma-Medica, Northridge, CA) The system comprises dual-head pixilated CZT detectors mounted on a modified mammographic gantry. For MBI, patients were injected with 296 MBq Tc-99m sestamibi and the standard CC and MLO views acquired of each breast. **Results:** A total of 98 patients with biopsy-proven breast cancer were enrolled and underwent preoperative MBI and completed surgical resection. MBI detected additional disease greater than that identified by the combination of mammogram and ultrasound which altered the surgical treatment in 12 patients (12/98 = 12.2%). In 7 of 98 patients, MBI detected additional foci of cancer not seen on mammography (7.1%). This resulted in change of surgical treatment plan from breast conservation to mastectomy. Final pathology confirmed that mastectomy was warranted. One patient (1%) had a contralateral breast cancer detected on MBI that was not detected with mammography. Second-look mammogram and ultrasound with biopsy demonstrated invasive breast cancer, and the patient underwent surgery on both breasts. Two patients (2%) had uptake in the contralateral breast on MBI. Surgical excision demonstrated atypical ductal hyperplasia and atypical lobular hyperplasia. Another patient had an abnormality detected on MBI which, at time of planned bilateral mastectomy, was found to represent atypical ductal hyperplasia. In 3 out of 98 patients, MBI detected a significantly greater extent of disease than mammography (3.0%) that resulted in change of surgical treatment plan from breast conservation to mastectomy. **Conclusions:** Molecular breast imaging can detect IDC, DCIS, and ILC, and can play a valuable role in evaluating extent of disease and presence of multifocal disease in the breast for surgical treatment planning.

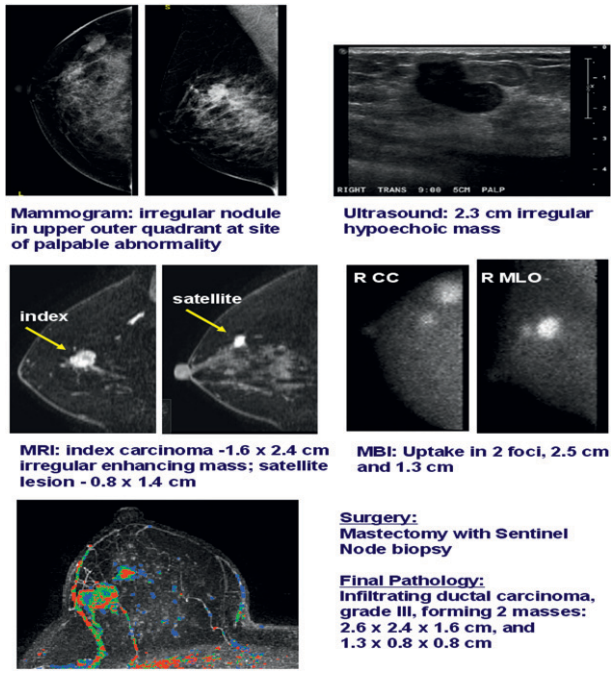

FIGURE 1. MBI detected additional focus of cancer. Mammogram: irregular nodule in upper outer quadrant at site of palpable abnormality. Ultrasound: 2.3 cm irregular hypoechoic mass. MRI: index carcinoma –1.6 × 2.4 cm irregular enhancing mass; satellite lesion –0.8 × 1.4 cm. MBI: uptake in 2 foci, 2.5 cm and 1.3 cm. Surgery: mastectomy with sentinel node biopsy. Final pathology: infiltrating ductal carcinoma, grade III, forming 2 masses: 2.6 × 2.4 × 1.6 cm and 1.3 × 0.8 × 0.8 cm.

26

Coregistered opto-acoustic and ultrasonic imaging for functional and anatomical maps of breast tumors. A.A. Oraevsky[1], D. Herzog[2], B. Clingman[2], S. Ermilov[1], V. Nadvoretskiy[1], A. Conjusteau[1], H. Brecht[1], R. Su[1], K. Kist[3], C. Dornbluth[3], O. Otto[3]; 1. TomoWave Laboratories, Inc., Houston, TX; 2. Seno Medical Instruments, Inc., San Antonio, TX; 3. University of Texas Health Science Center, San Antonio, TX

Objectives: Opto-acoustic imaging is rapidly emerging as a useful medical imaging modality with numerous clinical applications, including diagnostic imaging of breast cancer. The objective of this study was to evaluate feasibility of a multimodality opto-acoustic plus ultrasonic system, which provides optical contrast associated with tumor angiogenesis while mapping tissue structures with ultrasonic resolution. Optoacoustic images of blood distribution that provide functional information were obtained and superimposed with ultrasonic images showing morphological structures. Thereby, co-registered two-dimensional functional and anatomical maps of breast tumors were produced and employed to differentiate malignant from benign masses. **Methods:** The opto-acoustic system uses laser pulses in the near-infrared spectral range to illuminate tissues and detect the resulting ultrasonic pressure signals using a custom-made hand-held probe, which combines an array of ultrawide-band ultrasonic transducers and a fiberoptic light delivery system. Laser illumination at two wavelengths (757 nm and 1064 nm) provides contrast between hypoxic blood of breast carcinomas and normally oxygenated blood in benign fibroadenomas. Noninvasive diagnosis from combined opto-acoustic and ultrasonic images was compared with the gold standard of core biopsy. **Results:** A small blood vessel embedded in a breast tissue mimicking phantom was detected with high contrast and resolution at the depth of more than 5 cm. After the system was calibrated in phantoms mimicking the vasculature in the breast, a feasibility study was performed on female patients with breast masses having a BIRADS 4 score and who were scheduled for biopsy. Opto-acoustic maps, obtained at two different wavelengths, provided information for differentiation of breast carcinomas from benign tumors based upon differences in the optical absorption of hypoxic and normally oxygenated blood in the region of the tumor. In this pilot case study, the addition of opto-acoustic maps to ultrasound images qualitatively differentiated histologically benign tumors as benign and confirmed carcinomas. **Conclusions:** The opto-acoustic system developed by Seno Medical Instruments demonstrates that the depth of optoacoustic imaging is comparable with that of the breast ultrasound. The co-registration of an optically-induced functional contrast of blood and high resolution ultrasound imaging demonstrates the clinical feasibility of the multimodality system for diagnostic imaging of breast cancer as an adjunct to mammography. These early results suggest the need for a larger statistically significant study.

27

Near-infrared fluorescence imaging techniques for non-invasive lymphatic architectural and functional analysis. J.C. Rasmussen[1], I. Tan[1], M.V. Marshall[1], C.E. Fife[1], E.A. Maus[1], E.M. Sevick[1]; 1. University of Texas Health Science Center, Houston, TX

Objectives: To develop near-infrared (NIR) fluorescence imaging techniques to non-invasively assess lymphatic architecture and quantify lymphatic contractile function in control subjects and in subjects with breast cancer-related lymphedema. **Methods:** Each subject received multiple intradermal injections of microgram amounts of indocyanine green (ICG, total dose ≤400 μg ICG) in bilateral arms. Immediately following ICG administration, each subject was illuminated with a diffuse, 785 nm excitation light and the resultant 830 nm fluorescent signal was acquired using a custom-built, intensified charge coupled device (ICCD) camera imaging system. The resultant images were analyzed to assess lymphatic architecture and to quantitate the lymphatic contractile functional parameters of apparent lymph propagation velocity and period. **Results:** As shown below, distinct architectural differences were observed between the lymphatics of control subjects (Figure 1a) and the lymphatics of subjects with breast cancer-related lymphedema (Figure 1b). Propagation velocities and period were quantified and statistical models indicate that disease diagnosis has a significant effect ($p < 0.05$) on overall propulsion rate. **Conclusions:** NIR fluorescent imaging techniques can image and quantitate lymphatic contractile function in humans and may provide a means to assess the development and progression of lymphatic diseases such as metastasis and lymphedema.

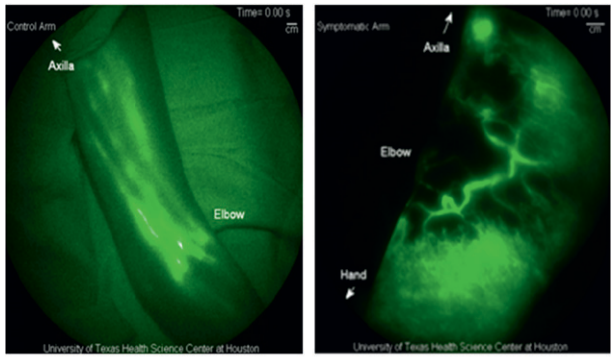

FIGURE 1.

28

Low-dose molecular breast imaging with Tc-99m sestamibi for screening in women with dense breasts. D.J. Rhodes[1], C.B. Hruska[1], R.W. Maxwell[1], A.L. Conners[1], M.K. O'Connor[1]; 1. Mayo Clinic, Rochester, MN

Objectives: We previously demonstrated that addition of Molecular Breast Imaging (MBI) to screening mammography (MG) significantly increased detection of node-negative breast cancer in dense breast from 27% with MG alone to 91% with the combination of tests ($p = 0.016$). This proof-of-principle study was performed with 740 MBq (20 mCi) Tc-99m sestamibi. After recent implementation of dose reduction methods for MBI, including optimized collimation and energy acceptance window, our objective is to compare performance of incident screen MG and prevalent screen low-dose MBI in 2400 women with dense breasts. **Methods:** Women presenting for screening digital mammography between June 2010–Jan 2011 who had heterogeneously dense or extremely dense breasts on past prior MG were enrolled. All participants underwent both MG and MBI. MBI was performed with 296 MBq (8 mCi) injection of Tc-99m sestamibi and dual head cadmium zinc telluride detectors and acquired in dynamic frames to allow generation of 148 MBq (4 mCi)-equivalent images. Mammograms and MBIs were read independently by 2 different radiologists. MBIs were assigned an assessment score of 1–5 which parallel BI-RADs; scores of 3–5 on MBI were considered positive and led to diagnostic workup. **Results:** In 440 women studied to date, 6 cancers were diagnosed in 6 patients. MBI detected cancer in 5 of 6 (83%) patients and MG detected none. The remaining cancer was detected on prophylactic mastectomy (7 mm invasive lobular carcinoma). Mammographically occult cancers detected by MBI included 2 cases of DCIS (6 and 15 mm), tubular cancer (7 mm) and invasive lobular carcinoma (36 mm). A total of 79 women were recalled for diagnostic evaluation of findings; 35 due to prevalent MBI alone, 40 due to incident MG alone, and 4 due to both tests. Eighteen women underwent biopsy; 16 prompted by MBI alone (PPV=25%) and 2 prompted by MG (PPV=0%). All 5 cancers detected by MBI were also visible on the 148 MBq (4 mCi)-equivalent images. **Conclusions:** Findings from this interim analysis indicate that low-dose MBI can be a useful adjunct and potential alternative to screening mammography in women with dense breasts. Follow-up mammogram at one-year for this cohort and further study of incident screening MBI will be necessary to establish true sensitivity and specificity. Ongoing dose reduction work will allow MBI screening to be performed with 74–148 MBq (2–4 mCi) Tc-99m sestamibi, with effective dose comparable to screening mammography.

29

Assessment of the advanced 3D registration for the spatial normalization of cross-sectional and longitudinal high-resolution breast PET/CT images. J. Santos[1], A.J. Chaushari[2], R.D. Badawi[2]; 1. University of California, Davis, CA; 2. UC Davis School of Medicine, Sacramento, CA

Objectives: To assess the performance of advanced 3D image registration (diffeomorphic demons) for normalizing cross-sectional pre- and post-contrast and longitudinal pre- and post-contrast high resolution (HR) breast CT scans. The former is necessary for improving the delineation of breast tumors and accurately estimating the volume. The later is for monitoring neoadjuvant chemotherapy (NAC) in human breast cancer patients through the use of HR PET/CT. **Methods:** Breast scanning was performed on a dedicated HR breast PET/CT scanner built at our institution. The CT resolution was 0.3 mm, isotropic. For registration, a non-rigid warping field was computed owing to interscan motion and repositioning errors using the diffeomorphic demons algorithm. The cost function was based on the maximization of mutual information and a multigrid approach was used for rapid computation. Registration was performed to warp the precontrast breast images to post-contrast ones at the same time point. Processing was repeated for longitudinal CT scans (acquired at baseline and after 2 cycles of NAC. The 3D warping field thus computed can be applied to the corresponding PET images. **Results:** When registering pre- to post-contrast scans, a visible decrease in error at the skin was observed due to spatial normalization when the diffeomorphic demons algorithm was used (see attached figure). Results were also compared with those obtained from mutual information based rigid body registration and improved performance was observed by the demons method. We are conducting an evaluation of the demons approach in a cohort of 10 breast cancer patients. **Conclusions:** Initial results indicate that the diffeomorphic demons method produced adequate performance for high resolution breast CT registration. It has potential to reduce radiologist burden and improve interpretation.

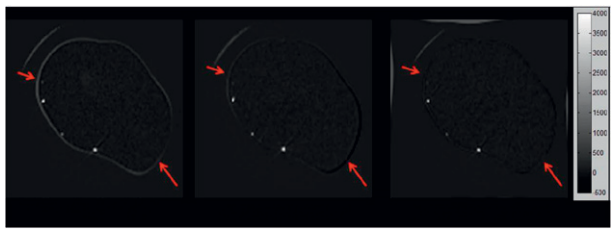

FIGURE 1.

30

Prediction of hormone insensitivity in women with metastatic breast cancer using estrogen PET (FESPET) discordance to glucose PET (FDG-PET) scans in comparison to primary tumor pathologic characteristics including Ki67 and HER2. K.S. Tonkin[1], A.A. Joy[1], S.K. Basi[1], D.W. Fenton[1], J.R. Mackey[1], J.O. Amanie[1], K. Tankel[1], S. Ghosh[1], J.L. Deschenes[1], A.J. McEwan[1]; 1. Cross Cancer Institute, Alberta, Canada

Objectives: The primary objective was to determine discordance between ([18F]-Fluorodeoxy-DGlucose) FDG-PET and (16a-[18F]-Fluoroestradiol) FES-PET scans performed prior to hormone therapy and subsequent response to hormone therapy. We determined the utility of pre-treatment FESPET scans in the prediction of response to first, second or third line hormone therapy in metastatic carcinoma of the breast. Another objective was to determine proliferative index and tumor aggressiveness as measured by immunohistochemistry (IHC) for Ki-67 and IHC and CISH (Chromagen In Situ Hybridization) for HER-2 respectively measured on the primary and correlated with metastatic disease response. The routine use of positron emission tomography (PET) scans utilizes the radiolabeled analogue FDG which is a glucose analogue. High tumor FDG uptake appears to be a predictor of poor outcome in individuals with large primary tumors or metastatic disease. Sixty percent of pre-menopausal and 80% of postmenopausal women have ER positive primary tumors. At first diagnosis of metastatic disease it is becoming more common to confirm ER positivity by biopsy or fine needle aspiration (FNA) of a single metastatic lesion. There are several functional PET tracers which image ER positive cells in breast cancer. The most widely reported of these is the FES PET scan. FES PET scans are positive in up to 80% individuals with primary tumor ER positivity. Where FDG and FES imaging has been undertaken in a single group of individuals' low FES uptake with high FDG is predictive of poor outcome and high FES uptake predicts better survival. Where metastatic tumors are ER positive the addition of FES to FDG PET could provide useful additional prognostic and/or predictive information with respect to treatment with antiestrogenic agents as in advanced breast cancer the level of FES uptake is predictive of response to hormonal therapy. Novel development: The study of FES-PET to determine applicability of hormone therapy for metastatic disease in women with primary tumor ER+ disease and the evaluation of PET results against IHC for ER, PR, KI-67 and IHC and CISH for HER-2 on the primary tumors. **Methods:** Patient inclusion criteria: Estrogen positive primary invasive ductal tumor on IHC; metastatic disease with or without loco-regional metastases; entered on study prior to initiation of first/second or third line hormone therapy for metastatic disease. Patient may be entered on a clinical trial of hormonal therapy in addition. Patients may have concurrent palliative radiation and bisphosphonates. Any previous adjuvant treatment is permitted. PET scan methods: Scans were done prior to first, second or third line therapy. FES and FDG scans were performed within 7 days of each other. FDG scans were performed with a Health Canada approved product according to Society of Nuclear Medicine procedure guidelines: http://interactive.snm.org/docs/jnm30551_online.pdf. FES was synthesized in house using a published synthesis pathway. Patients were injected with 5.2MBq/Kg FES and scanned on either a Philips or Allegro PET system. Images were acquired for 3 minutes per bed position, typically for 5 or 6 bed positions. Images were reconstructed and reviewed in coronal, sagittal and axial planes. Image review was double blinded to treatment and outcome using standard uptake values (SUV) and a tumor to background scale from 1=definitely negative to 5=definitely positive. Clinicians were only aware of the FDG results. The sites retaining hormone sensitivity (FES positive) were compared to FDG for each individual patient. In patients with widespread metastatic involvement up to 6 lesions were scored. Other radiology for staging purposes was done per clinician choice. Pathology methods: Primary tumor IHC studies for ER/PR were performed using a clinically validated assay in accordance with published guidelines (ER: Ventana SP1 clone, PR: PgR636 DAKO clone). Her2 neu was assessed using IHC and CISH, according to published guidelines (Dako polyclonal antibody 1/100). For HER2 2+/3+ CISH (Invitrogen HER2) was performed. Ki 67 was assessed using the MIB1 antibody (DAKO) at a dilution of 1/200, based on an in house technically validated protocol. Patient and Pathologic Characteristics: There were N=38; mean age was 53. Mean years from initial diagnosis to study entry (date of FES scan) is 9 years. Median is 8.5 years (range: 0.0 to 23 years). Adjuvant chemotherapy was given in 39.1% and adjuvant hormones were given in 36.8%; 24% received both adjuvant chemotherapy and hormone treatment. At initial diagnosis of breast cancer 42.1% were stage 2; 21.1%, stage 4; and 58% had liver/lung disease. The primary tumor was grade 2 in 50%. Lymphovascular invasion (LVI) was positive in 34.2%; 39.5%, 44.7% and 15.8% were starting first, second or third line hormones, respectively. ER 71% had 100% diffuse positive staining; 28.5% were 70–90% positive with N=1 patient low positive staining (>10% positive cells is considered positive). PgR 57.9% (N=22) had 60–100% staining, 26.3% (N=10) low positive (patchy <30–40% positive cells) and 13.2% (N=5) negative. HER2 3+ positive on IHC and/or CISH positive 26.3%. High Ki67 (≥15%) was seen in 50% (N=19) with all low Ki67 patients having HER 2 negative disease. **Results:** Thirty patients had evaluable data for FES and FDG scans, and clinical outcomes. FES showed fewer lesions in visceral/other sites compared to FDG; 67% (N=20) had discordance between Estrogen PET scanning and Glucose PET scanning (FES/FDG discordance) (Table 2); 20% (of the total N=30) had FDG +ve FES –ve lesions; 47% had a mixed pattern of FDG +ve and both FES +ve and FES –ve lesions. In the discordant group there was a significant correlation with high Ki 67 positivity (Pearson Chi square p=0.041). In the discordant group there was a significant correlation with HER2 positivity (Pearson Chi square p=0.006). At the initial follow-up evaluation Progressive Disease (PD) was seen in 50% of this discordant group. In this group there was PD on hormones in the site of discordance in 50% (N=10); 5 in liver ± other; N=1 in lung; N=4 in bone. Another 25% (N=5) had early progression but not in the discordant sites. For the remaining 25% their

TABLE 1
Patient Demographics (n = 38)

	n	%
Median age (years): At study entry (range)	66 (34–84)	
At initial diagnosis (range)	54 (27–80)	
Visceral disease		
Yes	22	58
No	16	42
Adjuvant chemotherapy:		
4 cycles	2	5.3
6–8 cycles	12	31.2
6 cycles and trastuzumab	1	2.6
No/missing	23	60.5
Adjuvant radiotherapy:		
Yes	23	60.4
No	13	34.3
Missing	2	5.3
Adjuvant hormones:		
Tamoxifen/AIs	14	36.8
No	16	42.1
N/A	1	2.6
Missing	7	18.4
Hormone treatment at study entry:		
1st line	15	39.5
2nd line	17	44.7
3rd line	6	15.8
Stage at initial diagnosis:		
Stage 1	11	28.9
Stage 2	16	42.1
Stage 3	3	7.9
Stage 4	8	21.1
Response to treatment:		
CR	2	5.3
PR	1	2.6
SD	17	44.7
PD	13	34.2
N/A or stopped early	4	10.5
Missing	1	2.6

TABLE 2
Outcomes in Relation to PET Scan Results (n = 30)

	FDG positive. FES positive	FDG positive. FES negative	FDG FES mixed
CR/PR	0	1	1
SD	7	3	5
PD	3	2	8

bone disease remained stable but these patients had discordance in non-bone sites and were being followed only by bone scans. In addition for 21% (N=8) FDG revealed unsuspected visceral disease and for N=4 patients the clinician chose to start chemotherapy rather than hormones directly as a result of the FDG-PET result. All 7 HER2 positive (6 did not respond to hormones) and 6 of 7 grade 3 cases were in the discordant group (p=0.01 for HER2 and p=0.05 for grade 3 (chi-squared)). CR+PR+SD vs. PD with Group 1 (High Ki67+low PR vs. others): Patients with high Ki67 and low or negative PR expression had an odds ratio=1.6 for PD (95% CI: 0.31–7.85) (p-value=0.593). CR+PR+SD vs. PD with Group 2 (High Ki67+low PR+ HER2 positive vs. others): Patients with high Ki67, low or negative PR and HER2 positive expression had an odds ratio for PD=1.4 (95% CI: 0.23–8.42) (p-value=0.713). Relationship of Ki67 with PR: Patients with highly positive PR expression were likely to have a low Ki-67 with an odds ratio=1.99 (95% CI: 0.49–7.94) (p-value=0.335). These odds ratios did not reach statistical significance, but are in the hypothesized direction and significance might be achieved with a larger sample size. **Conclusions:** 1. For practical reasons only a single metastatic lesion is biopsied to determine if metastases remain ER positive and likely to be hormonally responsive. At present optimum response determination for multiple lesions is unclear. 2. In this study 67% of the women had FDG/FES discordance, with fewer lesions on FES than FDG scans which predicted for disease progression at the first assessment after study entry in 50% of this group. Only 10% (N=3) patients with FES/FDG concordance had PD at the time of study analysis. 3. In addition for 21% (N=8) FDG revealed unsuspected visceral disease that required change to chemotherapy, as per clinician and patient choice, in N=4. 4. Thus FDG used with FES can predict hormone response and FDG-PET scans can avoid inappropriate hormone therapy for stage 4 metastatic breast cancer. 5. For the 7 patients with ER positive and HER2 positive primary tumors (likely Luminal B subtype) all showed FDG/FES discordance and 6 did not respond to hormone therapy. This group may not be suitable for hormone therapy alone but with such small numbers a larger data set would be required before making generalized statements. 6. The future impact of this study on breast cancer treatment would be to avoid inappropriate hormone therapy in the face of ER negative metastases defined by FES-PET scans enabling earlier use of chemotherapy treatment. 7. We plan to continue recruitment and biopsy FDG-positive/FES negative lesions to determine if they are pathologically ER negative. We will also determine PR, HER2, Ki-67 and review histological and molecular characteristics in comparison to the primary tumor.

31

A high-performance SPECT-CT system for dedicated molecular breast imaging. M.P. Tornai[1], R.L. McKinley[2]; 1. Duke University Medical Center, Durham, NC; 2. Zumatek, Inc., Research Triangle Park, NC

Objectives: To demonstrate the development, characterization and first clinical performance of a compact, fully-3D, patient friendly, quantitative, non-invasive, *in vivo,* hybrid molecular imaging SPECT-CT system dedicated to molecular breast imaging. **Methods:** Independent, high-performance SPECT and CT subsystems were developed, then hybridized onto a single platform having a common FOV to image the pendant, uncompressed breast. A contoured, comfortable, radio-opaque bed was developed for comfortable patient positioning. The SPECT sub-system is comprised of a CZT-based gamma camera with 2.5mm pixellation, intrinsic energy resolution of 6.7% FWHM and sensitivity of 39cps/MBq at 140keV; the system has fine polar, azimuthal and ROR motions facilitating dynamically controlled arbitrary trajectories anywhere in a hemisphere. The CT sub-system is comprised of a CsI digital flat-panel detector used with 0.5mm (binned) pixellation, and >80% sensitivity for the 36keV, 15% FWHM quasi-monochromatic x-rays from the cone beam x-ray source; the independent system has a fixed SID, and finely controlled polar and azimuthal motions allowing arbitrary trajectories in a banded spherical geometry. The volumetric sampling capabilities are demonstrated with sphere-loaded Defrise disk phantoms and arbitrary tilt angles. The 3D resolutions are evaluated. Human observer studies are used to evaluate the limits of detection with varying sized objects in geometric and anthropomorphic phantoms. Quantification of the SPECT includes attenuation and scatter correction of iteratively reconstructed data; CT quantification includes scatter correction. With IRB approval, several cancer-confirmed human subjects were imaged with fiducial markers either on SPECT, CT or hybrid SPECT-CT. **Results:** For SPECT: objects are reconstructed distortion free using fully-3D acquired data and iterative reconstruction, beyond the posterior breast; data quantitation is accurate to below 1.8kBq/mL; the smallest objects that could be statistically significantly reliably detected in an observer study had 35mL volume at 5:1 signal:background ratio; human images reveal focal uptake of tracer in surgically confirmed lesions, as well as in (surgically confirmed) DCIS in posterior breast; dual-modality fiducial markers help with image alignment and localization with CT image volumes. For CT: objects are reconstructed distortion free using fully-3D acquired data and iterative reconstruction; the smallest spherical objects detected with statistically significant difference relative to mammography were 34mL in volume; scatter correction facilitated image attenuation coefficients to within 5% of narrow beam values; measured CT doses in cadaveric breast samples were <4.5mGy; human subject images revealed clearly distinguishable disease in 3D and with high resolution. **Conclusions:** This sensitive, high performance,

dedicated breast imaging system has high diagnostic, and potentially screening, utility.

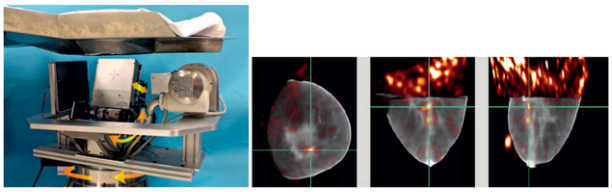

FIGURE 1.

32

A high resolution, high sensitivity PET camera dedicated to breast imaging. A. Vandenbroucke[1], F. Lau[1], P.D. Reynolds[1], D. Innes[1], J. Zhai[1], C.S. Levin[1]; 1. Stanford University, Stanford, CA

Objectives: Positron emission tomography (PET) has shown to be a valuable modality in breast cancer management, despite the limited sensitivity and spatial resolutions of the cameras currently being used in the clinic. PET systems have been proposed to aid breast cancer detection by resolving inconclusive mammograms, especially in younger, radio dense breasts, as well as to enhance staging capabilities and to enable accurate monitoring of response to therapy. **Methods:** Our goal is to build a 1 mm^3 resolution, high sensitivity clinical PET camera. Improving the sensitivity enables shorter acquisition times, higher patient throughput, and/or a lower administered dose. Higher spatial resolution allows the detection of smaller lesions and hence an earlier and more accurate diagnosis. High sensitivity is achieved by placing the camera heads close to the breast (figure A), employing thick detector volume, and packing the crystal elements tightly together: 147,456 crystal elements are packed in each 164.6×93.6×20 mm^3 head (figure B and C). High resolution is obtained using miniscule scintillation crystals (1 mm^3), which convert the 511 keV photons emitted from the patient into optical light. In addition, detecting optical photons on the sides of the crystal rather than at the ends ensures localization of the 511 keV photon interactions in all 3 dimensions (figure C), enabling an accurate estimate of the first interaction as well as its incident angle, allowing significant imaging improvements. **Results:** Detector tests showed a point-spread function of 0.837±0.049 mm (figure D), a coincident time resolution of 6.71±0.03 ns FWHM, and a 511 keV photopeak energy resolution of 10.9±0.1% FWHM using our in house developed electronics, including all cabling and connectors that will be used in the final system. Reconstructed image slices of a simulated phantom indicate that 2 mm diameter lesions can be reliably detected in 15 seconds, based on an activity ratio of 10:1, 4 cm panel separation and a background activity of 37 kBq/ml. Simulations also showed that implementing 5 mm thick shielding around the camera reduces background counts by 45%. **Conclusions:** A 1 mm^3 resolution, high sensitivity breast camera is under development. System performance studies indicate that excellent spatial, energy and temporal resolutions are achieved and small lesions can be rapidly detected. We believe that these features will increase the role of PET in breast cancer management and make it more practical for the clinic.

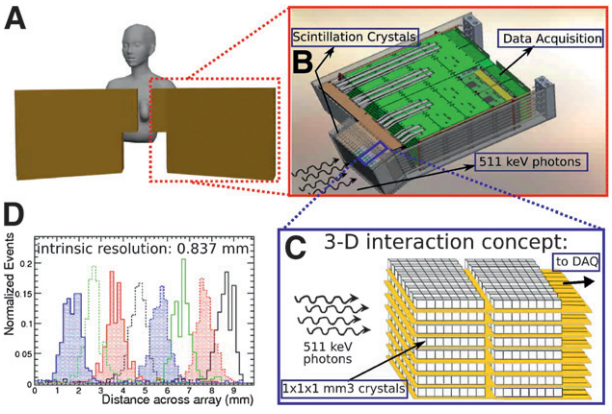

FIGURE 1.

33

Low-dose molecular breast imaging in radiographically dense breasts. D.J. Wagenaar[1], J.W. Hugg[1], R.A. Moats[2], S. Chowdhury[1], B.E. Patt[1]; 1. Gamma Medica, Inc., Northridge, CA; 2. Children's Hospital of Los Angeles/USC, Los Angeles, CA

Objectives: Molecular Breast Imaging (MBI) uses 99mTc sestamibi for detection of breast cancer, especially in women with radiographically dense breast tissue. High diagnostic accuracy has been reported in 1000 patients, with sensitivity equivalent and specificity generally superior to that of DCE-MRI. Our objectives are: 1) to optimize an MBI system for low-dose and 2) to compare the benefit/risk from MBI with mammography, tomosynthesis, PEM, and BSGI. **Methods:** MBI uses two digital solid-state (CZT) gamma cameras to mildly compress the breast and obtain conjugate images in standard CC or MLO views. We combine the two images and apply denoising filters to increase system efficiency. In addition, we optimized the detector pixel size and collimation for two-camera MBI. The registered parallel square-hole collimator aligns each detector pixel with a collimator hole, and the pixel pitch is optimized for geometric efficiency. The collimator length is optimized for lesion detectability (>1 mm) in the proximal half breast viewed by each camera. Acquisition time is 5–10 minutes per view, or 20–40 minutes for CC and MLO scans of both breasts. Increases in detection efficiency are traded for reductions in injected radioactivity and/or scan time. **Results:** The new dual-camera MBI system with registered collimators (1.6 mm pixel pitch) improves detection efficiency by a factor of 3.6. Recommended injected radioactivity is now reduced from 20–30 mCi to 8 mCi in clinical practice. Ongoing studies aim to verify that injected doses of 2–4 mCi provide high diagnostic accuracy. Risk from a 2–4 mCi injection is equivalent to that from a 4-view mammography study. Benefit/risk ratios for MBI equal mammography and exceed tomosynthesis, PEM, and BSGI. **Conclusions:** MBI is an alternative to DCE-MRI in women with dense breast tissue. The radiation risk has been lowered into the range of mammographic screening. Further potential improvements in system efficiency and, hence, dose-reduction have been identified.

34

Cost-effective molecular breast imaging in emerging countries. I.N. Weinberg[1], P. Stepanov[1], V. Zavarzin[2], W.J. Ryder[3]; 1. Weinberg Medical Physics LLC, Bethesda, MD; 2. A&D Precision, LLC, Newton, MA; 3. Portsmouth Hospitals NHS Trust, Portsmouth, UK

Objectives: The mainstays of large-scale breast cancer detection in the Western world (i.e., x-ray mammography) are inappropriate for emerging countries, primarily due to the high cost of biopsies associated with false-positive imaging findings [see microsimulation by QL Okwonko, et al. Breast Cancer Screening Policies in Developing Countries: A Cost-effectiveness Analysis for India. JNCI 2008;100:1290–1300]. Imaging specificity (and concomitant reduced unnecessary biopsy rate) could be increased with the addition of molecular breast imaging. We wished to investigate the design of a low-cost high-confidence system (aimed at emerging countries) that would incorporate both molecular imaging and x-ray tomosynthesis. **Methods:** Monte-Carlo simulations were performed to examine the count-efficiency of positron emission mammography (PEM) detectors, used in combination with a moving x-ray source/detector pair that would shuttle along with the PEM detectors, to produce laminographic x-ray images. PET imaging experiments were conducted with silicon photomultipliers (SiPMs), to assess the ability of multiplexing to reduce overall cost of the system. A microsimulation model [*supra*] was employed to assess the costs-per-life-year-saved in an emerging country using the proposed system. **Results:** X-ray laminography was demonstrated with the moving x-ray detector pair. Multiplexed readout PEM detectors demonstrated 2-mm spatial resolution, with sparse SiPMs array. The microsimulation predicted a ten-fold decrease in dollars per life-year saved as compared to x-ray mammography, and a three-fold decrease as compared to clinical examination alone, with approximately 10,000 breast-cancer deaths averted per million participants as compared to either of these modalities. The microsimulation assumed market costs for FDG in large Indian cities. New radiotracers employing Ge-68 generator systems under investigation could reduce costs further. **Conclusions:** Low-cost co-registered PEM/x-ray

tomosynthesis systems would save lives at lower costs in emerging countries than conventional imaging or clinical breast examination.

35

Clinical use of a stereotactic breast-specific gamma imaging apparatus in the localization of breast lesions for biopsy. B.L. Welch[1], C. Lorino[2], D. Chiarella[2], T. Hodge[2]; 1. Dilon Technologies, Newport News, VA; 2. Montgomery Breast Center, Montgomery, AL

Objectives: Breast-Specific Gamma Imaging (BSGI) is a molecular breast imaging technique which is increasingly being used in the diagnostic workup of breast patients and has demonstrated the ability to detect cancers missed by mammography and ultrasound. A stereotactic lesion localization apparatus has been developed to allow BSGI-guided vacuum-assisted needle biopsy (GammaLōc, Dilon Technologies Inc.). The purpose of this work is to present the results of the clinical performance of this system on a small group of patients. **Methods:** Patients who were indicated for needle biopsy based on clinical findings of an abnormality on BSGI conducted as part of their clinical workup were imaged and the area of concern localized on the GammaLōc Apparatus. All patients were injected with 20–30 mCi of Tc99m-Sestamibi and imaging was initiated within 10 minutes post injection. The breast was placed in light compression for stability and two stereotactic planar images were acquired at (+) and (–) 20°. Using software, the lesion was located in each stereo view and X, Y and Z coordinates were calculated. The resulting location was correlated to a specific X, Y location within the localization grid in the paddle and a depth from the needle guide. A special gamma emitting obturator was used to verify proper localization prior to conducting biopsy. **Results:** Twenty three patients have been imaged and the lesions identified. The localization, correlation and verification steps described above were conducted for all lesions. Resulting pathology was compared to the other clinical evidence to determine concordance or discordance. This work presents several case examples including clinical imaging and the results of pathology. **Conclusions:** The GammaLōc Stereotactic lesion localization apparatus provides a clinically viable, convenient method for localizing lesions seen in BSGI. This device promises to address an important limitation to broad acceptance of this imaging technique by allowing accurate lesion localization and biopsy under the guidance of this molecular breast imaging technique.

36

Scanner for dual modality breast tomosynthesis. M.B. Williams[1], Z. Gong[1], P.G. Judy[1], K.L. Klanian[1], T.H. Patel[1], O.P. Sullivan[1], S. Soni[1]; 1. University of Virginia, Charlottesville, VA

Objectives: Molecular imaging of breast cancer using dedicated cameras for radiotracer distribution mapping is an effective means of obtaining functional information that is complementary to the structural information of x-ray mammography. We have developed a hybrid breast scanner designed to provide molecular images that are congruent in form with the anatomic images of x-ray breast tomosynthesis (XBT). The objective is to obtain XBT and molecular breast imaging tomosynthesis (MBIT) scans in quick succession, permitting reconstruction of 3-dimensional structural/functional breast images. **Methods:** The dual modality tomosynthesis (DMT) scanner is an upright unit in which the XBT and MBIT subsystems rotate around a common axis. The breast support can be independently rotated to perform mild breast compression in any desired direction. The x-ray subsystem uses a high output tungsten target tube with external rhodium filtration, and a CsI(Tl)–CMOS detector. The gamma camera uses parallel hole collimation and a pixelated NaI(Tl) crystal array optically coupled to an array of position sensitive photomultiplier tubes. MBIT reconstruction is done via an EM algorithm constrained by an XBT-derived mask matrix describing the location of the breast surface. A cylindrical ray-driven projector-backprojector is incorporated to reduce artifacts due to the asymmetrical and undersampled acquisition process and to permit partial resolution recovery. **Results:** The DMT scanner has undergone pilot clinical evaluation. Seventeen women with a total of 21 biopsied lesions were scanned using Tc-99m-sestamibi prior to biopsy. An observer study was performed to determine the added value of including MBIT with XBT for lesion detection and characterization. Histopathological results were taken as ground truth. Of the 21 lesions, 7 were determined by biopsy to be malignant and 14 were determined to be benign. The sensitivity, specificity, positive predictive value, negative predictive value and accuracy of DMT scanning were 86%, 100%, 100%, 93%, and 95%, respectively, compared to 86%, 57%, 50%, 89%, 67% for XBT alone. We also report on the scanner's measured physical performance characteristics, including x-ray detector DQE, and gamma camera resolution, sensitivity, and uniformity of response. **Conclusions:** Our experience to date suggests that DMT scanning is a feasible and accurate method for breast cancer detection and diagnosis and that specificity and positive predictive value can be improved through the addition of MBIT to XBT.

37

Translational molecular imaging of breast cancer. K. Zhang[1], C. Intenzo[1], S. Kim[1], B. Cavanaugh[1], A. Frangos[1], C. Dascenzo[1], E. Wickstrom[1]; 1.Thomas Jefferson University, Philadelphia, PA

Objectives: VPAC1 encodes G-protein coupled receptors that are expressed, irrespective of their hormonal status, on all breast cancers at the onset of the disease. The receptor concentration is more than 1000 fold greater than on the stroma or the epithelial cells. The objective was to target VPAC1, with a receptor-specific Cu-64 peptide probe for PET imaging of breast cancer. **Methods:** A 33-mer peptide was synthesized with GABA as a spacer and diaminodithiol (N2S2) as a chelating agent covalently bound at the carboxy terminus. Association constants were determined, and preclinical tissue distribution and PET imaging studies were performed in immunocompromised female mice bearing MCF-7 human breast cancer tumors (n=10). Receptor specificity was determined by receptor blocking studies (n=10). Imaging of spontaneous breast cancer in transgenic MMTVneu mice (n=9) was also performed using F-18-FDG as a control. Tumors were extirpated for histology and to determine VPAC1 expression by RTPCR. Autoradiography was performed using human breast cancer biopsy specimen and adjacent tissue (n=10). Following eIND, toxicology and radiation dosimetry studies, the probe, Cu-64-TP3805, was then used for an ongoing feasibility study in humans with breast cancer. **Results:** The chemical purity of TP3805 was > 97% at Kd value $3.3\times10\text{-}9$ M. Radiochemical purity averaged 97±2%. In mice, the tumor/blood ratios were 2.54±0.25% and 3.67±0.09%, and tumor/muscle ratios were 9.18±1.09% and 7.67±2.32% at 4 hr and 24 hr post injection. In MMTVneu mice, eight spontaneous tumors confirmed by histology were imaged by Cu-64-TP3805 but only four of these were visualized with F-18-FDG. RTPCR confirmed VPAC1 expression in all eight lesions. In addition, two lesions determined to be benign by histology and which did not express VPAC1 receptors were seen by F-18-FDG but not with Cu-64-TP3805. In autoradiography, the Cu-64-TP3805 uptake averaged 5.9±0.5%. In patients (n=6) all lesions were detectable with Cu-64-TP3805. No adverse events were noted. Further work is in progress. **Conclusions:** Cu-64-TP3805 promises to be a specific and promising agent for imaging breast cancer in humans.